POLITECNICO DI TORINO

Department of Environment, Land and Infrastructure Engineering

Environmental and Land Engineering Master's Degree

Design and implementation of tests to verify feasibility of different remediation technologies at a complex petrochemical site

Supervisor:

Prof. Tiziana Anna Elisabetta Tosco

Co-Supervisors:

Laura Simone, team lead environmental restoration Arcadis

Dr. Monica Granetto

Master's Degree's Thesis of Mitra Hossein Pouri

Academic Year 2023-2024

Abstract

BTEXs are prevalent contaminants at petrochemical sites, posing significant environmental and health risks due to their toxicity and mobility in soil and groundwater. This thesis examines the use of a commercial colloidal activated carbon (CAC) as an injectable reactant in the form of a water-based colloidal suspension, which is injected into the contaminated aquifer forming a treatment zone, and acts by adsorbing the BTEX present in groundwater, immobilizing them. The applications of CAC in environmental remediation are increasing in number thanks to its high surface area and strong adsorptive capacity. Conducted under the supervision of the Groundwater Engineering Group at Politecnico di Torino and Arcadis in Germany, this research included laboratory tests aimed at assessing the CAC colloidal stability and mobility in porous media, identifying 1 g/l as the optimal concentration for testing. Experiments were also conducted with NaCl added in varying concentrations to investigate the effects of ionic strength on colloidal stability, aggregation behavior, and adsorption efficiency. Additional tests were performed in deionized water (DIW) as well as in tap water. The analytical techniques adopted for the characterization of the CAC suspensions included scanning electron microscopy (SEM), CPS disc centrifugation, dynamic light scattering (DLS), ultraviolet-visible (UV-Vis) absorption spectroscopy. Column tests were conducted to study the CAC mobility in the porous medium.

The first analysis focused on the characterization of the CAC particles in terms of morphology and size, revealing that the studied CAC is predominantly composed of 0–50 μm particle size range. This first finding is potentially promising for its application in groundwater remediation since small size corresponds to a favorable surface area-to-volume ratio (facilitating effective BTEX adsorption) and expected good mobility in the porous medium. These preliminary hypotheses allowed to consider the studied CAC as a potential candidate for the field application, and therefore the following stages of the laboratory tests were aimed at verifying these hypotheses. Further characterization revealed that increasing NaCl concentrations the average particle size (Z-average) increases, with great variability at higher concentrations. This suggests that particle aggregation is occurring in the presence of salts, which may pose a potential issue for the application in aquifer systems characterized by a high salt content. Conversely, the CAC suspensions in DIW were observed to maintain a good colloidal stability at lower concentrations, with particle aggregation likely occurring at higher concentrations. Sedimentation tests showed a decreasing trend in C/C_0 over time,

suggesting that the formation of aggregates leads to a (at least partial) sedimentation. Finally, column test results revealed a partly limited mobility in the porous medium. in columns 10 cm long, less than 10% of CAC was recovered at column outlet, with most retained in the upper portion of the column. To conclude, the studied commercial CAC shows promising for in-situ BTEX remediation. The partly limited colloidal stability and mobility in the porous medium on the one hand may represent an issue for the preparation of CAC suspensions in the field, their injection and effective delivery in the target area (with a likely limited radius of influence) but, on the other hand, they may represent a positive aspects since they would guarantee that, once injected and delivered in the target treatment zone, the particles will not re-mobilize easily, thus preventing long-term re-mobilization of the adsorbed BTEX.

Contents

List of figures

List of Tables

1. Introduction

The oil industry, while achieving many successes, has also shown significant environmental drawbacks over time. Its operations—such as extraction, refining, transportation, and storage—have caused extensive contamination, impacting ecosystems, communities, and natural resources. Oil spills, leaks, and runoff pollute water bodies, while improper disposal contaminates soil, making it unsuitable for agriculture and disrupting ecosystems. Soil contamination from oil can last long-term, posing health risks to workers, nearby communities, and wildlife through exposure. Groundwater, a vital freshwater source, is especially vulnerable, underscoring the need to address contamination risks seriously.

In addition to the general types of contamination associated with the oil industry, there are specific contaminants of concern that merit attention due to their persistence, toxicity, and widespread occurrence. This work focused in particular on BTEX (Benzene, Toluene, Ethylbenzene, and Xylenes, a group of aromatic hydrocarbons commonly found associated to petrochemical sites (Yu et al. 2022).

The specific petrochemical site under investigation in this study is situated in North-West Germany, proximate to a river vital for the city's water supply (*figure 1.1*). The primary objective is to immobilize and eliminate the BTEX contaminants from the site through the implementation of remediation technologies, with a concurrent focus on preventing their downstream transfer to the river. The remediation method employed utilizes a specific type of colloidal activated carbon (CAC) as a water-based colloidal suspension. This injectable reactant is introduced into the contaminated aquifer to create a treatment zone. Through this method, CAC effectively absorbs contaminants present in the groundwater, trapping them within its porous structure.

figure 1.1. Site location, (Google Map, 2024)

The research initiative was conducted under the joint supervision of Politecnico di Torino and Arcadis company Germany. The study was divided into two distinct phases, encompassing both the research component and on-site visits in partnership with the company. Additionally, laboratory tests were carried out in collaboration with Politecnico di Torino. The tests involved the characterization of CAC, by means of scanning electron microscopy (SEM), CPS disc centrifugation, dynamic light scattering (DLS), ultraviolet-visible (UV-Vis) absorption spectroscopy, and column testing to study the mobility of the CAC suspensions in porous media. These tests assessed particle size, CAC content, material and metal composition, particle size distribution via sedimentation, as well as the stability, and mobility of CAC within a porous medium.

This thesis is structured into four main chapters following the initial introduction, which provides a general overview of the main themes and the study.

Chapter 2 presents the literature review, a detailed review of the properties of BTEX, their behavior in groundwater, and the specific challenges posed by remediating BTEX contamination at petrochemical sites. The CAC technology will be described, including its mechanism, advantages, and limitations in application. Additionally, there will be a brief overview of conventional remediation methods, along with a comparison between these methods and CAC technology.

Chapter 3 provides a detailed description of the site, covering site details such as geology, hydrology, prior investigations, groundwater characterization, and current contamination levels. Chapter 4 describes the experimental methods adopted for the laboratory tests conducted,

identifying all factors influencing CAC characteristics for subsequent analysis. It also presents the laboratory test results with graphical representations for clarity and analysis, including findings on the optimal CAC dilution and additional tests using NaCl, DIW, and tap water. Lastly, Chapter 5 offers the final conclusions of the study.

2. Literature Review

At petrochemical sites, groundwater contamination represents a significant environmental issue, primarily due to the release of hazardous substances during operations, accidental spills, or improper disposal. BTEX—a group of volatile organic compounds (VOCs) comprising benzene, toluene, ethylbenzene, and xylene—are of particular concern because of their widespread presence in petroleum products such as gasoline and crude oil. These compounds are notable for their toxicity, persistence, and mobility in groundwater, making them challenging to manage, especially in complex hydrogeological settings (Wang et al. 2022). This review synthesizes research on the properties, environmental behavior, and remediation challenges associated with BTEX compounds. Furthermore, it assesses conventional remediation technologies and explores the advantages and limitations of colloidal activated carbon (CAC), a novel technology with promising applications for complex hydrogeological settings. Through this review we highlight knowledge gaps in BTEX remediation and support the case with continued research into CAC's effectiveness.

2.1. Chemical and Environmental Characteristics of BTEX Compounds

As shown in figure 2.1, each BTEX compound has unique chemical characteristics that influence its behavior in the subsurface environment and its associated risks (Anjum et al. 2019).

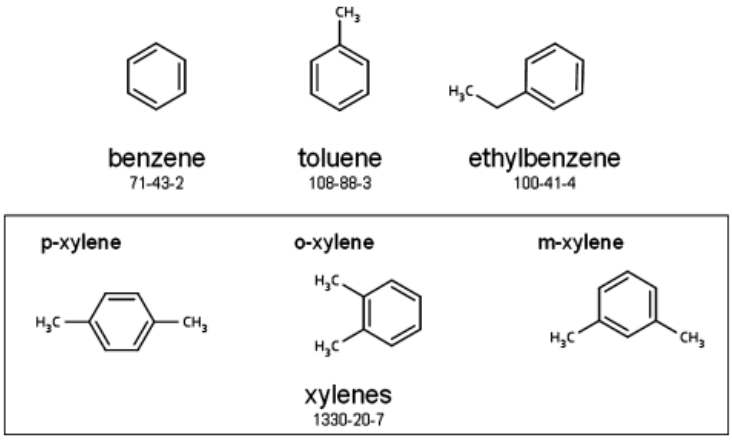

figure 2.1. BTEX chemical structure (Fayemiwo, Om & Daramola, M.O. & Moothi, Kapil, n.d.)

Also, the table below provides an overview of the physical and chemical characteristics of BTEX compounds.

Compound	Formula	Molecular Weight	Boiling Point (°C)	Solubility in water at room temperature (ppm)	Density (g/ml)	Vapor pressure (torr)
Benzene	C_6H_6	78.11	80.1	1780	0.88	75
Toluene	$C_6H_5CH_3$	92.1	110.8	515	0.87	22
Ethyl-benzene	$C_6H_5CH_2$-CH_3	106.17	136	152	0.87	7
O-xylene	C_6H_4-$(CH_3)_2$	106.17	144.4	175	0.88	6

Table 2.1. Physical and chemical properties of BTEX compounds (Merck Index 1989, Yong and Rao 1991, and Cheremisinoff 1992)

Benzene is classified as a priority pollutant by regulatory agencies due to its carcinogenicity. It is both highly toxic and highly mobile. It dissolves easily in water, which allows it to spread rapidly through groundwater systems. Chronic exposure to benzene has been linked to serious health issues, including leukemia, which necessitates stringent control measures at contaminated sites (IARC Monographs Volume 120, 2018).

Toluene is less toxic than benzene, but still poses significant risks to human health and ecosystems ("World Soil Day," n.d.). It has moderate solubility in water, making it fairly mobile in groundwater systems. However, it is somewhat more biodegradable than benzene, which can make it less persistent in some conditions (National Center for Biotechnology Information, 2024)

Ethylbenzene is known to cause respiratory irritation and other adverse health effects. It is less soluble in water than benzene or toluene, but it can still migrate through groundwater, particularly near petrochemical facilities (National Center for Biotechnology Information, 2024). Its potential to volatilize also contributes to risks related to vapor intrusion into buildings (U.S. Environmental Protection Agency (EPA),2015).

Xylene (o-, m-, and p-Xylene) is comprising several isomers. It is less soluble than benzene and toluene, but it remains toxic, particularly to the central nervous system. Due to its frequent use in petrochemical processes and its widespread presence in fuel, xylene contamination is common in groundwater near industrial sites (National Center for Biotechnology Information, 2024). Like other BTEX compounds, xylene is often introduced into the environment through spills, leaks, or improper waste handling.

2.2. Transport and Degradation of BTEX in Groundwater

The fate of BTEX in groundwater is governed by their physical and chemical properties, as well as subsurface environmental factors. These compounds' ability to dissolve, migrate, volatilize, and biodegrade varies, affecting how they interact with soil, water, and air in contaminated environments (Wang et al. 2022b).

BTEX compounds are moderately soluble in water, which allows them to dissolve into groundwater and spread from the contamination source. They move with groundwater, following the natural flow patterns of the aquifer. This enables them to contaminate large areas, often spreading far beyond the initial contamination site (Wang et al. 2022b).

The table below presents an example of water solubility and concentrations of BTEX compounds found in gasoline.

BTEX	Water solubility /mg L^{-1}	Gasoline concentration (% v/v)
Benzene	1740-1860	2-5
Toluene	500-627	6-7
Ethylbenzene	131-208	5
Xylenes	167-196	6-7

Table 2.2. Water solubility and concentrations of BTEX compounds in Gasoline ("Water-Solubility-and-Common-Concentrations-in-Gasoline-of-BTEX.Png (712×183)," n.d.)

The hydrodynamic processes, namely advection and dispersion influence the distribution of BTEX in aquifers. Advection transports the dissolved contaminants along with groundwater flow, while dispersion, refers to the spreading of the contaminants both along and across the primary flow direction, influenced by heterogeneities in the aquifer at both the small (pore-scale) and large (regional-scale) levels ("The Handbook of Groundwater Engineering. Pdf," Jacques W. Delleur, 1999).

Also, BTEX compounds are volatile, meaning they can volatilize into the atmosphere when exposed to air. In shallow groundwater or near the water table, this volatility can lead to the migration of BTEX into the vadose zone (the unsaturated zone above the groundwater) and eventually into buildings, posing a risk of vapor intrusion (Costa et al. 2012).

2.3. Challenges of BTEX Remediation in Complex Hydrogeological Sites

BTEX remediation is particularly challenging due to the complexities of the subsurface environment, which often impact the effectiveness of both conventional and advanced remediation technologies.

One major issue is the heterogeneous nature of the subsurface. Heterogeneities in soil composition, permeability, and groundwater flow result in irregular contamination plumes that may be difficult to map and remediate effectively (Li et al., 2024).

Additionally, non-aqueous phase liquids (NAPLs) commonly found at petrochemical sites act as persistent sources of contamination. Density defines the behavior of NAPLs in the subsoil as LNAPL (Light NAPL), density lower than water density and DNAPL (Dense NAPL), density higher than water. In the unsaturated zones, the LNAPL and DNAPL flow down displacing air in the pores (imbibition). Even when the spill stops, the NAPL remains as residual saturation, dissolved in water and in pore air. Despite the low solubility of the LNAPL and DNAPL, they slowly dissolve in water forming the contaminant plume ("The Handbook of Groundwater Engineering. Pdf," Jacques W. Delleur, 1999). Even when remediation efforts reduce dissolved-phase concentrations, these residual NAPLs continue to release hydrocarbons into the groundwater even over decades, prolonging the contamination (Li et al., 2024).

Another significant complication arises at shallow sites where volatilization of BTEX compounds can lead to vapor intrusion into nearby buildings, posing health risks. Remediation must address not only

groundwater contamination but also the migration of harmful vapors into the indoor or outdoor air (Han et al. 2024).

Moreover, the rebound effect presents a recurring challenge. This phenomenon is often observed after the stopping of pump-and-treat systems: contaminants that seem to have been removed during initial remediation often resurface as the plume re-equilibrates, thus, necessitate prolonged monitoring and, in many cases, additional remediation efforts (O'Connor et al., 2018).

2.4. Comparison of Conventional Remediation Methods

Groundwater remediation at petrochemical sites involves several conventional techniques, such as pump-and-treat, air sparging, and bioremediation (Yu et al. 2022). These methods have been widely applied in the past to address contamination, including volatile organic compounds (VOCs) like BTEX. However, these techniques often face significant limitations, particularly in complex petrochemical sites with challenging hydrogeological conditions and the presence of non-aqueous phase liquids (NAPLs). Below is a summary of these traditional methods and their limitations.

Pump-and-Treat is one of the most traditional groundwater remediation techniques. The method involves extracting contaminated groundwater using wells (pumping) to the surface and then treating it above ground using technologies like activated carbon filtration, air stripping, or chemical oxidation to remove contaminants before discharging it or reinjecting it into the aquifer (Ciampi et al. 2023a).

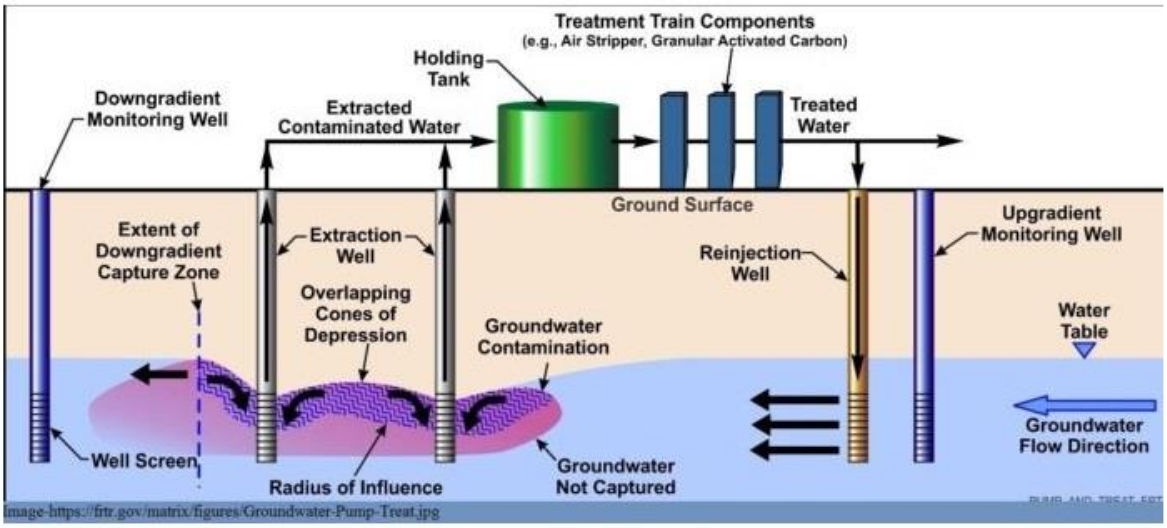

figure 2.2. Remediation of contaminated sites-the Pump and Treat ("Remediation of Contaminated Sites-The Pump and Treat System | Wealthy Waste" 2022)

Despite its long history of use, pump-and-treat has several significant drawbacks, especially in complex hydrogeological settings such as slow process, incomplete treatment, limited effectiveness in complex hydrogeology (Ciampi et al. 2023b).

In a case study from Vienna, Austria, a former manufactured gas plant site was contaminated with pollutants such as PAHs, hydrocarbons, phenols, BTEX, and cyanide, posing significant environmental risks. The chosen remediation strategy involved excavating the core contaminated areas and installing a hydraulic barrier to protect the surrounding aquifer, with on-site treatment of extracted groundwater. A pilot-scale treatment plant was operated for six months to design the foreseen pump-and-treat system. The scope was to test the effectiveness of different process steps, which included an aerate sedimentation basin, a submerged fixed film reactor (SFFR), a multi-media filter, and an activated carbon filter. The system demonstrated significant efficiency, removing over 99.8% of contaminants like PAHs and BTEX, with all treated water meeting Austrian legal standards for discharge. The initial concentrations of BTEX (295 – 806 µg/l) and of benzene (247 – 547 µg/l) were removed by 100%. However, the study also highlighted the necessity of pre-treatment to address issues like clogging from tar and sulfur compounds. The results indicated that a combination of physical, biological, and chemical methods was essential to meet regulatory discharge standards and not only one remediation system can afford the target individually. (Wirthensohn et al. 2009).

Also, a comparative study carried out in 2010, which analyzed the field data obtained in 10 gas stations in the city of Porto Alegre, Brazil for 4 years showed that the pump-and-treat method (in combination with a SVE unit) was the most efficient to remove BTEX and TPH (Almeida et al. 2019), (Caetano et al. 2016).

Air Sparging is another in situ remediation technique that involves injecting air into the subsurface to volatilize and remove contaminants, from groundwater. It is often combined with soil vapor extraction (SVE), which removes the volatilized contaminants from the vadose zone (unsaturated zone above the water table). While air sparging can be effective for BTEX compounds, it has several limitations, especially in complex petrochemical sites (Oh, Namgung, and Kim 2024).

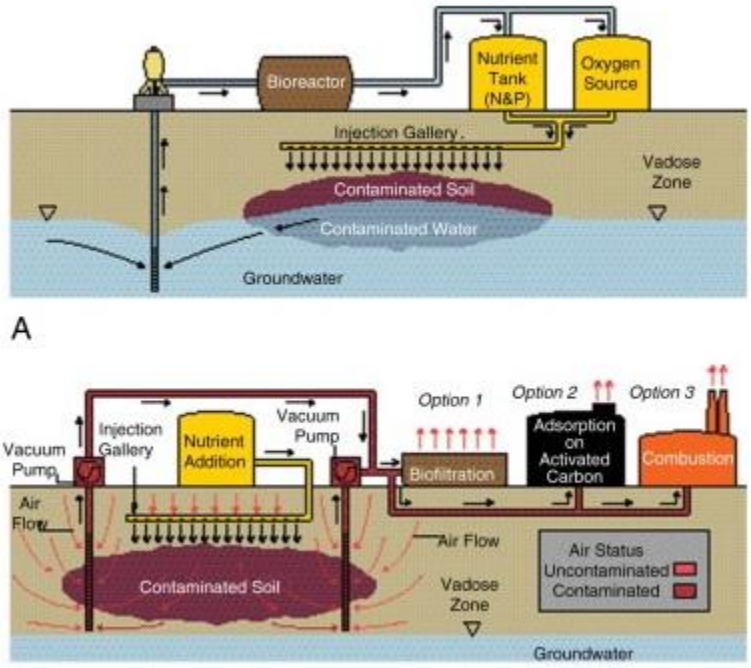

figure 2.3. Air sparging mechanism ("Air Sparging - an Overview | ScienceDirect Topics," n.d.)

In the USA (1997), sites contaminated with gasoline and initial benzene levels varying between 3 mg/l and 600 mg/l were treated by air sparging. Removal rates ranging between 59% and 99% were reached within 5 to 30 months. Initial BTEX levels of 6 mg/l and 24 mg/l fell by 68% and 95% within 3 to 24 months (EPA – United States Environmental Protection Agency, September 1997).

In 2004, a study reviewed the soil and water remediation systems. The paper (Khan, Husain, and Hejazi 2004) presented the results obtained with field-scale air sparging in combination with SVE. BTEX levels in a gas station in Florida, USA, fell from 24,000 µg/l to 10 µg/l during 47 months (a 99.9% decrease). In another case, in a gas station in New Hampshire, USA, the concentration of BTEX decreased from 3270 µg/l to 5 µg/l (99.8%) within 13 months.

The table below provides a brief comparison of the two remediation technologies described before, highlighting their mechanisms, strengths, and limitations.

Method	Mechanism	Strengths	Limitations
Pump-and-Treat	Physical removal	Effective for initial contaminant reduction	High energy cost, limited efficacy in heterogeneous aquifers
Air Sparging	Volatilization	Suitable for shallow contamination	Limited in clayey/low-permeability soils

Table 2.3. Comparison of conventional BTEX remediation techniques

Given these limitations, innovative or combined technologies such as colloidal activated carbon (CAC) are being explored to address the shortcomings of traditional approaches and to enhance contaminant capture and in situ treatment at complex sites.

2.5. Colloidal Activated Carbon (CAC)

Colloidal Activated Carbon (CAC) is a remediation technology designed to mitigate groundwater contamination by leveraging the adsorption properties of activated carbon in a colloidal form, particularly at complex petrochemical sites. CAC technology is based on the properties of activated carbon, which is known for its high surface area and strong adsorptive capacity. The technology is

particularly well-suited for addressing BTEX and other hydrocarbon contaminants commonly found in groundwater near petrochemical facilities (Molé et al. 2024).

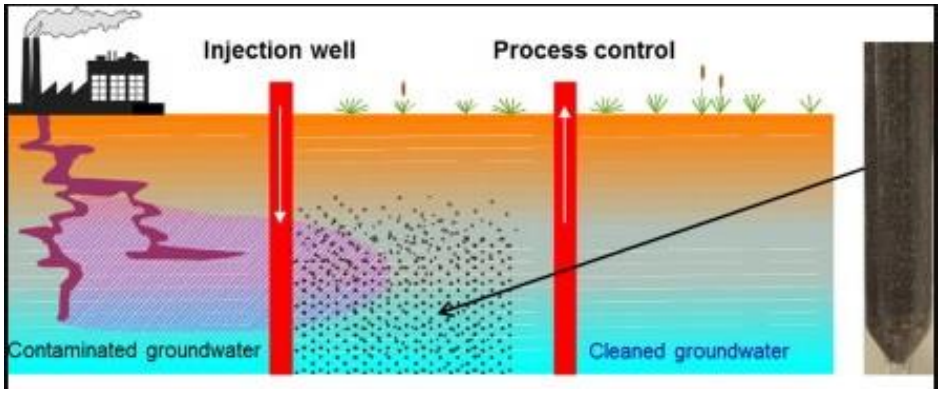

figure 2.4. Installation of sorption zones by injection of CAC (Georgi et al. 2015a)

The credit to develop commercial activated carbon goes to a Swedish chemist von Ostreijko who obtained two patents, in 1900 and 1901, on covering the basic concepts of chemical and thermal (or physical) activation of carbon, with metal chlorides and with carbon dioxide and steam, respectively (Bhatnagar et al. 2013).

The key scientific principle behind the efficacy of activated carbon in removing contaminants from groundwater is adsorption, a process by which contaminants bind to the surface of activated carbon through physical forces and hydrophobic interactions (Georgi et al. 2015b).

Activated carbon is widely recognized for its high adsorption capacity, largely due to its porous structure, which provides extensive surface area for contaminant adsorption. It is produced from a variety of carbonaceous rich materials such as wood, coal, lignite and coconut shell (Bhatnagar et al. 2013). Oxygen, hydrogen, sulfur and nitrogen are generally present in activated carbon in the form of functional groups and/or atoms chemically bonded to the structure (Bhatnagar et al. 2013).

Moreover, activated carbon has a high surface area, typically in the range of 10–200 m2/g (Hu and Srinivasan 2001).

Table 2.4 is a detailed comparative table analyzing Colloidal Activated Carbon (CAC) against Granular Activated Carbon (GAC) and Powdered Activated Carbon (PAC), focusing on adsorption capacities, distribution characteristics, and cost-effectiveness.

Parameter	Colloidal Activated Carbon (CAC)	Granular Activated Carbon (GAC)	Powdered Activated Carbon (PAC)
Adsorption Capacity	High initial adsorption, effective for low-to-moderate contaminant concentrations in situ due to colloidal size	High adsorption capacity, suitable for concentrated point sources or ex situ applications	High surface area provides excellent adsorption but may not sustain for long-term containment in situ
Particle Size and Distribution	Colloidal-size particles (0.5-2 μm) allow even distribution in groundwater and access to small pores	Larger particles limit (~0.5-2.5 mm) distribution in fine soils, but effective in high-flow areas and filtration systems	Fine powder (10-100 μm) disperses well but can be difficult to control in situ, leading to clogging in some porous media
Injection Feasibility	Easy to inject and disperse in situ, effective for permeable reactive barriers in aquifers	Difficult to inject; typically used in above-ground filtration systems or trenches	Challenging to inject due to fine size and can require stabilizers for even dispersal
Cost-Effectiveness	High initial cost but low maintenance due to long-term in situ containment	Moderate cost with extensive maintenance required for regeneration or replacement	Low cost but high maintenance due to frequent need for reapplication in dynamic environments
Reusability and Longevity	Limited reusability; typically stays in place for long-term adsorption without significant desorption issues	Often regenerated in ex situ applications, adding to operational costs	Non-reusable, typically applied once; high potential for adsorbent saturation and faster breakthrough
Application Suitability	Best for in situ applications with complex, heterogeneous groundwater flow	Primarily ex situ or point-source treatments in permeable media, less suitable for large, dispersed plumes	Often used in short-term or emergency spill response due to rapid adsorption, less ideal for sustained remediation

Table 2.4. Comparison table of different activated carbon forms

Colloidal Activated Carbon (CAC) involves the use of highly dispersed activated carbon particles suspended in water or another carrier fluid (McGregor 2020). In comparison to other forms of activated carbon, such as granular activated carbon (GAC) and powdered activated carbon (PAC),

CAC offers unique advantages in subsurface remediation ("Activated Carbon Manufacturing Plant Project Report 2024," n.d.). Unlike GAC, which is typically used in above-ground treatment systems like filter beds, CAC is injected directly into the contaminated subsurface, where it creates a permeable reactive zone that absorbs contaminants from groundwater as it flows through it by the natural flow, reducing their mobility and concentration in the groundwater. (Plagentz et al., 2006, USEPA, 2002). Thus, CAC enables it to treat contaminants in situ, especially in areas where groundwater flow and soil heterogeneity make traditional methods less effective. CAC remains relatively immobile once injected due to its particle size and interaction with subsurface soil, allowing for more controlled treatment of contamination plumes over time.

The key advantage of CAC lies in its ability to provide a high surface area for adsorption while being adaptable for injection into complex hydrogeological settings, making it an ideal solution for managing persistent organic pollutants at petrochemical sites where other technologies may struggle to reach contaminants in low-permeability zones or fractured bedrock (McGregor 2020).

The figure below captures the main visual comparison, focusing on the differences in particle sizes and the types of activated carbon: granular activated carbon, powdered activated carbon, and colloidal activated carbon.

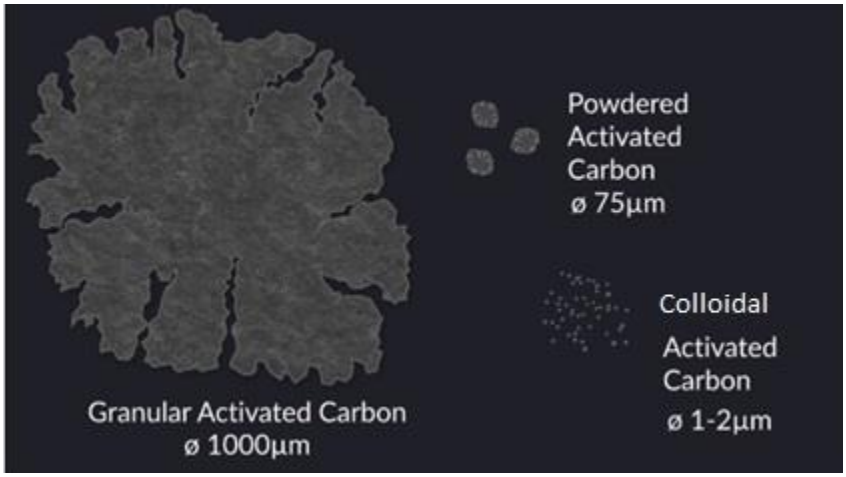

figure 2.5. Particle size comparison of activated carbon types (Sterkenburg 2020)

Installation of carbon-based injectates (CBI) can be done using direct-push technology (DPT) or other methods in practically any geological setting, from sandy aquifers to low-permeability zones

and weathered or fractured rock when high-energy injection techniques are employed. Many variables must be determined before going to the field, including injection point grid spacing (both areal and vertical) across the target treatment zone, injection technology, pressure and injection flow rate, the mass of AC product to be injected at each depth and location, and top-down versus bottom-up injection technique (Noland and Winner 2024).

The spacing between injection points should be adjusted based on geological setting, project goals, and costs. High-pressure injection is commonly used to facilitate emplacement of CBIs in heterogeneous systems by creating preferential, and thus a heterogeneous distribution of the colloidal material around the injection points (Noland and Winner 2024).

During injection, the CAC follows the path of least resistance (Noland and Winner 2024) and, due to physical and chemical interactions, sedimentation, or mechanical filtration, it deposits onto the soil matrix, becoming immobilized in the subsurface. Deposition of CAC on the sediment creates a sorption barrier against further spreading of hydrophobic pollutants (Georgi et al. 2015b).

As mentioned before, the primary mechanism through which CAC operates is adsorption. When contaminants such as BTEX encounter activated carbon particles, they adhere to the carbon surface due to a combination of physical and chemical interactions (Bergler et al. 2013). These interactions are driven primarily by the hydrophobic nature of BTEX compounds, which causes them to partition out of the aqueous phase and onto the non-polar carbon surface (Georgi et al. 2015).

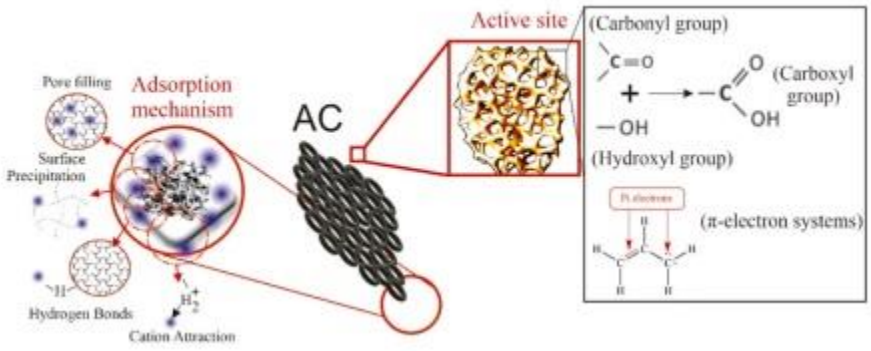

figure 2.6. The adsorption mechanism on the surface of activated carbon (Heryanto et al. 2024)

Many functional groups like phenol, carboxyl, and carbonyl have responsibility for the outer surface of carbon to improve its adsorption performance because they act as a molecular binder for pollutants (Heryanto et al. 2024).

Furthermore, CAC has several important properties that make it an effective tool for groundwater remediation. Its small particle size provides an exceptionally large surface area, which enhances its ability to adsorb contaminants, even when present at low concentrations (Hu and Srinivasan, 2001). Additionally, CAC has a high affinity for hydrophobic organic contaminants, such as BTEX, which preferentially adsorb onto the carbon surface rather than remaining dissolved in groundwater (Hu and Srinivasan, 2001).

To mention some projects of using activated carbon, a laboratory study analyzed the performance of different amounts of AC used as adsorbent in the treatment of water contaminated with crude oil and petroleum in Eagle Island, Port Harcourt, Nigeria. Efficiency was measured based on TPH (Total Petroleum Hydrocarbons, a large family of several hundred chemical compounds that originally come from crude oil) levels ("Total Petroleum Hydrocarbons (TPH) | ToxFAQs™ | ATSDR," n.d.). The results showed that the method removed 99.9% of TPH (with initial and final concentrations of 9,304.70 mg/l and 12.37 mg/l) (Ayotamuno et al. 2006).

In another case study, a former gasoline retail station located in Whitby, Ontario, was the site of BTEX and PHC (are comprised of a broad range of thousands of different chemical compounds that originate from naturally occurring geological sources including crude oil, bitumen, natural gas and coal) ("Petroleum Hydrocarbons," n.d.) contaminants requiring remediation. Excavation, as well as pump and treat approaches, had been used to address contaminant levels, but groundwater remained impacted by BTEX and PHC F1(this fraction contains hydrocarbon chains from C6 to C10) and F2 (this fraction contains hydrocarbon chains from C10 to C16.) above regulatory ("PHC Testing," n.d.). While the contractors were able to remove the majority of impacts, they were not able to remediate the site to the applicable regulatory standards. Using a proprietary design, the contactor injected CAC, to remediate residual BTEX and PHC F1 and F2 groundwater impacts. The remedial program was completed in two days with the first clean samples obtained within three weeks of post-injection. The BTEX and PHC plumes were treated below the regulatory standards. Sampling has been performed over four quarters and the site has been deemed remediated ("PlumeStop-Remediation-Toronto-Canada.Pdf," n.d.).

2.6. Advantages and Limitations of CAC

Colloidal activated carbon (CAC) presents several advantages over conventional remediation methods like pump-and-treat and air sparging. One significant benefit is its in-situ application, which involves directly injecting CAC into the subsurface, allowing for treatment of contaminants in place without the need for large-scale excavation or ex-situ treatment facilities. This makes it particularly attractive for sites with limited access or deep contamination (Global NEST Journal, Vol 10, No 1, pp 54-61, 2008).

Additionally, once applied, CAC requires minimal operational oversight. Unlike pump-and-treat systems, which must be operated continuously, CAC remains in the subsurface and continues to adsorb contaminants passively over time (Carey et al. 2024).

Despite its advantages, CAC technology has certain limitations that must be considered. Its finite adsorption capacity means that over time, the carbon particles can become saturated with contaminants. In high-contamination scenarios, additional injections of CAC may be required to maintain effectiveness. However, this can increase the overall cost of remediation, particularly for large-scale areas (Niarchos et al. 2023). There is a remote risk that, over time, CAC particles could become remobilized, potentially carrying contaminants with them through the aquifer. If the contaminants have not been broken down or treated effectively during this period, this movement could spread pollution in an uncontrolled manner.

Another challenge is competitive adsorption. In cases where multiple contaminants are present, such as BTEX compounds alongside chlorinated solvents, there may be competition for adsorption sites on the carbon surface. This could reduce the overall efficiency of CAC in removing target contaminants (Niarchos et al. 2023).

Finally, while CAC offers a passive, in site remediation solution, long-term monitoring is essential to ensure that contaminants remain adsorbed and that there is no desorption or rebound of contaminants into the groundwater. Regular monitoring ensures that CAC continues to function effectively over time (Almpanis, Slater, and Power 2024).

3. The Contaminated Site

3.1. Site Description

Arcadis' client manages a fuel depot at the investigated Site (hereafter referred to as "Site"). Contamination of Arcadis' client property, involving BTEX and TPH (C10-C40), has been detected in both the soil and groundwater. The soil contamination was first identified in 1987 during construction work near the filling station area. Following this, the site was subjected to systematic investigations. Since 1987, whenever contaminated soil was discovered during various construction projects, the affected soil was replaced as part of excavation activities conducted for structural purposes.

In 1991, groundwater remediation and containment efforts commenced using a pump and treat (P&T) system, along with oil skimming and continuous groundwater monitoring. In 2016 and 2017, the P&T system was temporarily shut down to implement further active measures, including field tests with surfactants and nitrates, as well as a full-scale nitrate-based treatment. These actions were intended to reduce the residual contamination at the source, thereby limiting the spread of the pollutant plume.

A 2019 feasibility study evaluated various alternative methods for remediating and containing the pollutant plume, identifying the injection of colloidal activated carbon (CAC) as the optimal solution. This approach aimed at creating an adsorption zone across the entire cross-section of the aquifer, effectively stopping the discharge of pollutants through groundwater. After the pump and treat (P&T) system was decommissioned, the CAC injection was implemented in 2019. Although pollutant concentrations initially decreased after the injection, a subsequent rapid rise led to the recommendation of a follow-up CAC injection.

Arcadis did not design or implement the colloidal activated carbon (CAC) injection system for this project. Their role was limited to reviewing its effectiveness and assessing the need for future injections. They concluded that additional injections would not benefit the site.

3.2. Location

The property spans approximately 4,200 m^2 and includes several tank containers for the storage and distribution of mineral oils, such as: four above-ground tanks in the southern section (two 100 m^3

heating oil tanks, one 50 m^3 diesel tank, and one 60 m^3 diesel tank), two underground 100 m^3 tanks in the eastern area, a multi-chamber tank with a total capacity of 30 m^3 in the northern part, and a single tank, likely holding 20 m^3, in the central area. Additionally, several decommissioned tanks are located beneath the platform in the central area. Other structures on the property include a gas station, a social building, a large office building, a warehouse, and various smaller storage and office facilities. The entire area is covered with blacktop, paving, or concrete surfaces.

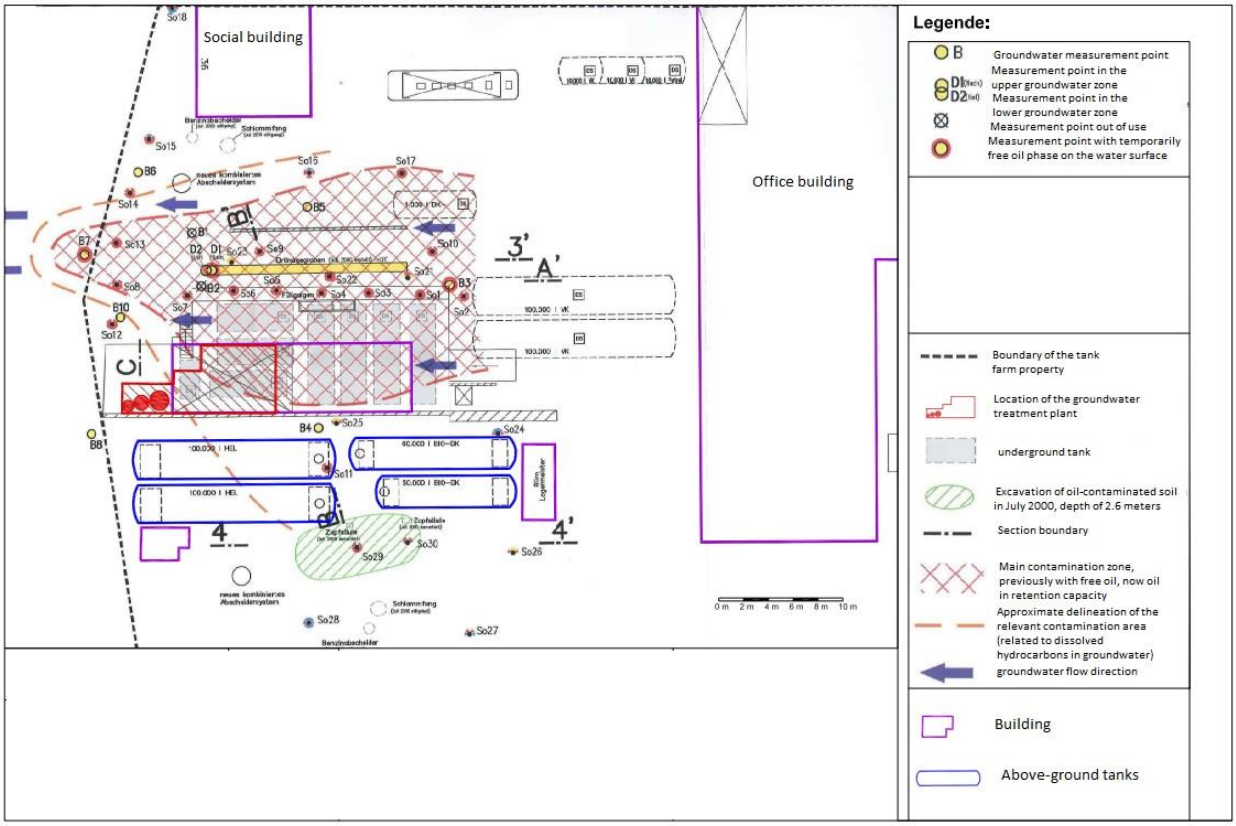

figure 3.1. Site map (Arcadis report)

3.3. Geology and Hydrogeology

The soil structure at the site can be described as follows:

Fill: This layer consists of a heterogeneous mixture of gravel and sands, occasionally containing silt and stones. It extends from the surface to approximately 0.6 meters below ground level, with

maximum depths reaching up to 4 meters. For compacted fills, the hydraulic conductivity may be low, around 10^{-7} to 10^{-9} m/s, while more granular fills may have higher values (Woessner and Poeter 2020).

Flood loams: These are sandy soils, sometimes containing clay and humus, and reach depths of up to 1.1 meters below ground level, with maximum depths up to 2 meters. The hydraulic conductivity, ranging from 10^{-6} to 10^{-8} m/s (Panagos et al. 2014)

Fine sands: Extending to about 7.5 meters below ground level, these soils can reach depths of up to 8 meters and may contain localized deposits of medium and coarse sands, as well as silt layers in lens- and horizon-like formations. The hydraulic conductivity is ranging from 10^{-4} to 10^{-6} m/s depending on their level of compaction and sorting.

Fine sandy, slightly clayey silt: This layer begins at around 7.5 meters below ground level, with a maximum depth of 8 meters, and is characterized by fine sandy soil with a slight clay content. The hydraulic conductivity is around 10^{-7} to 10^{-8} m/s.

These soil characteristics provide critical information about the geological composition and hydrogeological conditions of the site, which are essential for evaluating groundwater flow, contaminant migration, and remediation strategies.

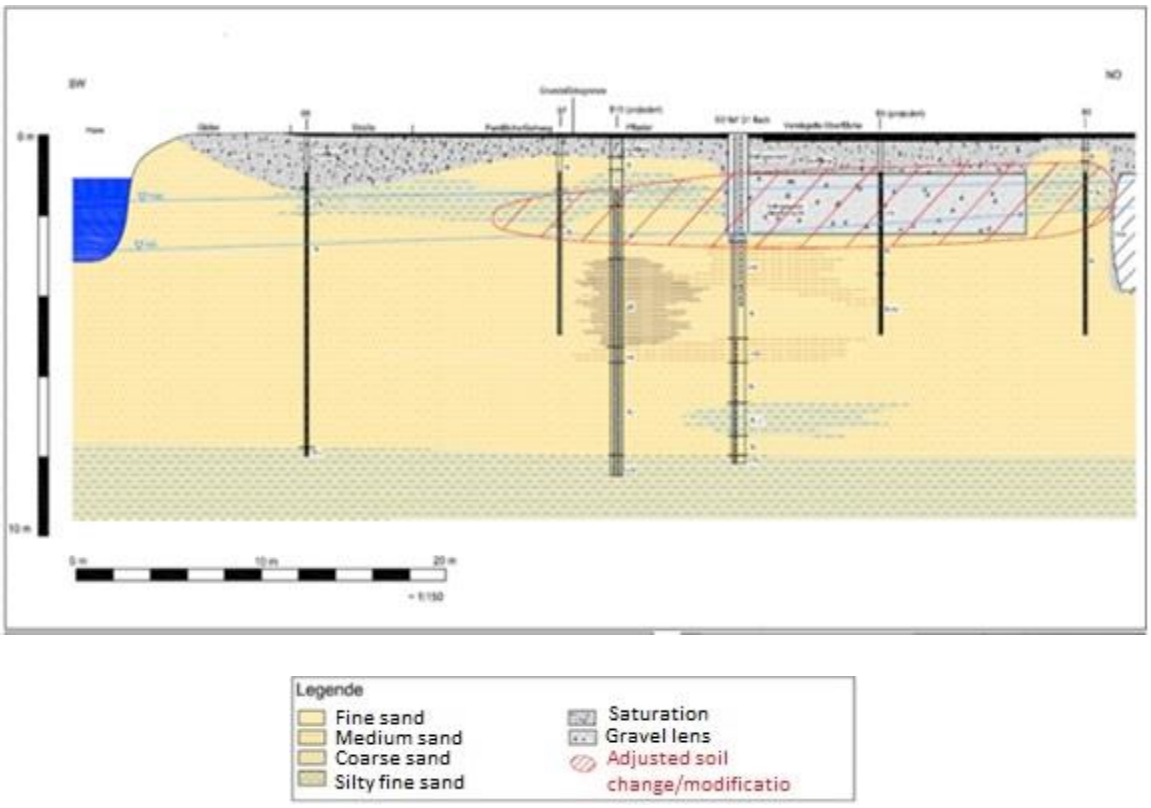

figure 3.2. Geological section in groundwater flow direction (Arcadis Report)

The fine sandy, slightly clayey silts at a depth of approximately 7.5 to 8.0 meters below ground level act as the main groundwater-bearing layer. The groundwater table fluctuates seasonally, typically between 1.2 meters and 2.6 meters below ground level. However, the presence of a low-permeability flood loam layer causes partial confinement of the groundwater.

The hydraulic conductivity of the porous aquifer varies based on the silt content in the sands. Pumping tests have shown hydraulic conductivity ranging from 7.8×10^{-6} m/s to 2.6×10^{-4} m/s. Groundwater flow on the site is predominantly towards the southwest to west, eventually discharging into the nearby river, which flows north-northwest and receives groundwater from the site (*figures 3.3 and 3.4*).

Based on the horizontal hydraulic gradient derived from the 2018 equipotential map, with an average of around 0.3%, the estimated average groundwater flow velocity is approximately 0.1 m/day (based on Arcadis report).

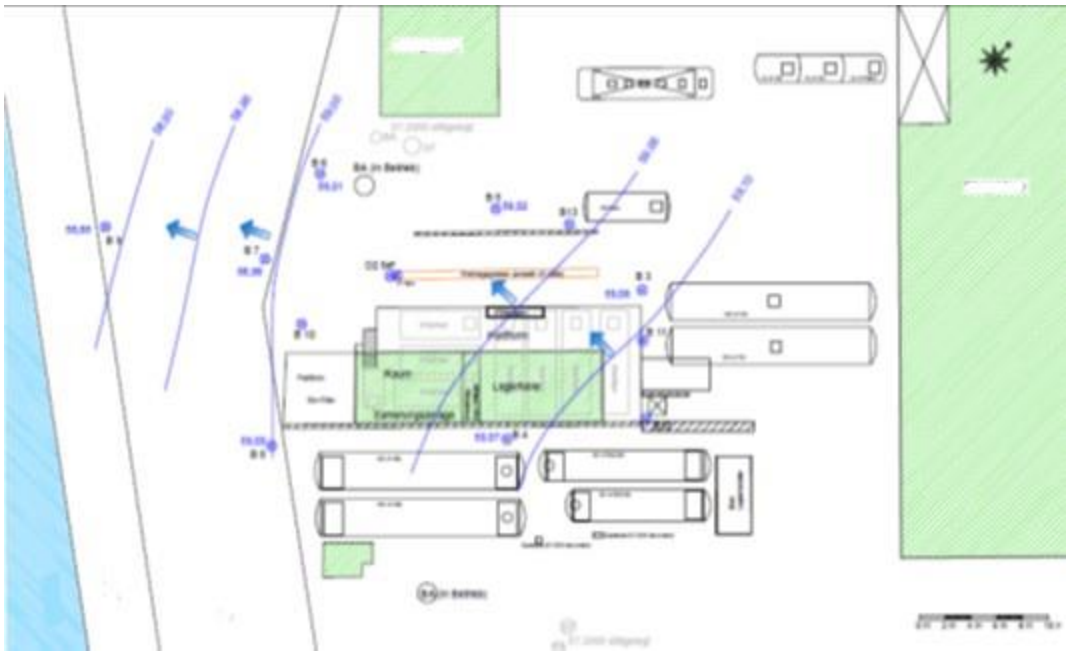

figure 3.3. Groundwater flow direction in March 2018(Arcadis Report)

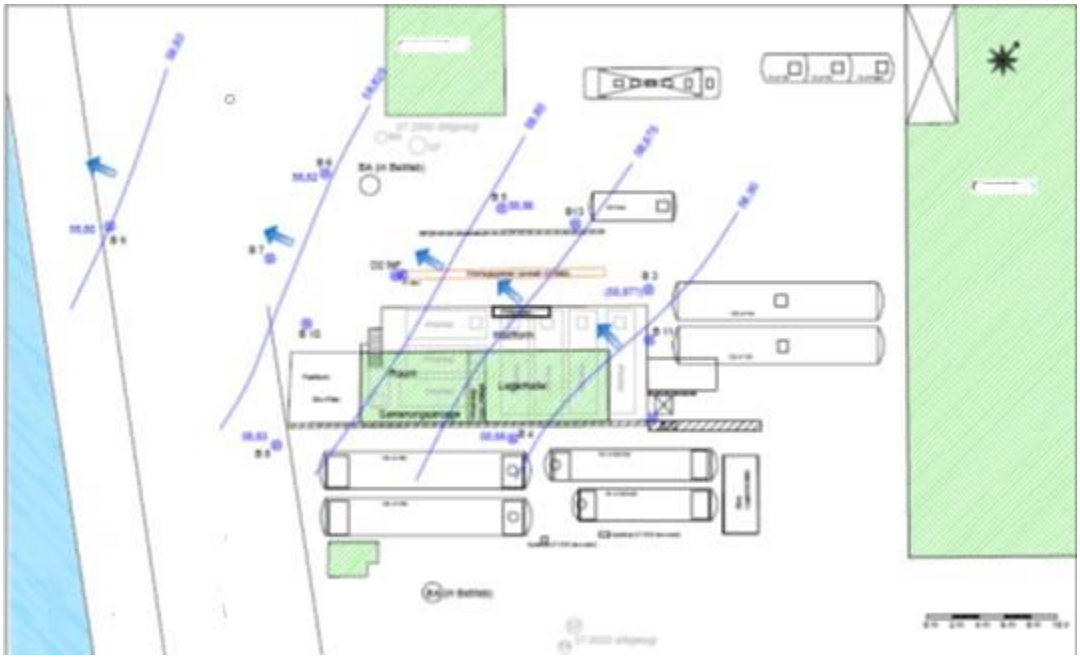

figure 3.4. Groundwater flow direction in October 2018(Arcadis Report)

3.4. Groundwater Characterization

The timeline of key events and activities related to groundwater exploration and monitoring at the site is as follows:

- **1987:** Initial site exploration
- **2009:** Establishment of groundwater monitoring point B10.
- **March-May 2009:** Pumping tests were conducted,
- **September 2009 onwards:** Groundwater monitoring was conducted every 1-2 months at points B6 - B10
    - Minimal changes in pollutant concentrations were observed during remediation work pauses.
    - Significant pollutant levels were found at B3, B4, B5, and B7, while B6, B8, B9, and B10 showed little to no contamination
- **2017:** Installation of additional groundwater monitoring points B11, B12, and B13

3.5. Current Contamination Status

The most comprehensive groundwater sampling occurred in October 2018, with further monitoring from 2019 to 2021 to assess the effectiveness of the colloidal activated carbon adsorption zone. However, only selected monitoring points with different parameter ranges were analyzed.

3.5.1. Pollutant Distribution – October 2018

The October 2018 sampling focused on BTEX concentrations. The highest concentrations, ranging from 887 µg/l to 1,390 µg/l, were found near the filling station and decommissioned tank containers beneath the platform (B3, B4, and remediation well D1). Downstream, concentrations decreased to 133–364 µg/l (B13 and B5), and further downstream, BTEX levels fell below detection limits, except for B7, which showed 131 µg/l. The elevated concentration may suggest an additional contamination source, or a pollutant shift during the 8-month remediation system shutdown (March-November

2017). No detectable BTEX levels were found at the railway tracks in October 2018 (B9). Upstream of the main contamination area (B11 and B12), BTEX concentrations remained low, below 10 µg/l.

3.5.2. Pollutant Distribution – April 2021

Sampling, conducted in April 2021, focused on benzene concentrations only, revealing a significantly different distribution compared to October 2018. In the main contamination area, benzene concentrations ranged from 1,200 to 3,750 µg/l, considerably higher than in 2018. Downstream areas (B5, B7, B10) also showed a marked increase in benzene levels. Notably, benzene concentrations at B10 rose to 550 µg/l (compared to near detection limits in October 2018), and at B9, concentrations increased to 29 µg/l.

3.6. Remediation and Safety Measures

3.6.1. Soil Remediation Measures

Soil replacement activities were conducted in conjunction with various construction projects at the site between 1988 and 2000. These projects included upgrades to the filling station, the construction of a retaining wall, the installation of liquid-tight roadways, and the renewal of separator systems. Contaminated soil encountered during these works was excavated and removed, to the extent that structural conditions allowed.

3.6.2. Groundwater Remediation Measures

The groundwater remediation efforts to date can be summarized as follows:

- **April 2009:** Groundwater extraction was halted to convert the drainage shaft into a well with filters at two depths (D1 and D2), followed by monitoring without extraction.
- **August 2011:** The remediation plant was recommissioned, with the following measures:
    - Extraction water from D1 at a rate of 0.5 m^3/h.

    - Groundwater monitoring at B6 – B10, with intervals extended to approximately every six months.
    - Installation and maintenance of oil-binding fleece in B3 and B7.
- **March 22, 2017:** Temporary shutdown of remediation plant for field tests involving surfactants and nitrates.
- **November 28, 2017:** Restart of the system after field tests.
- **September 2019:** Shutdown for the injection of colloidal activated carbon downstream.

During extraction from well B1, the floating oil phase was also skimmed and collected via an oil separator. In addition to the phase skimming at well D1, oil-binding fleece was installed at B3 and B7, which was replaced during maintenance and monitoring activities.

Between May 1991 and September 2018, a total of 5,078 liters of LNAPL were removed from the aquifer. The majority of this recovery occurred during the first nine years of remediation (1991-2008), with about 5,000 liters extracted during that period. From 2008 onward, only small amounts of oil, or none at all (between 2014 and 2018), were recovered annually. As of 2018, measurable amounts of LNAPL were detected in D1, B5, B7, and B13.

A total of approximately 36.7 kg of BTEX was removed from the aquifer during the operational period from August 2011 to January 2019.

In 2016, based on laboratory tests, a field trial using a nitrate solution was conducted. The input was made to groundwater measuring point B3. It is reported that a notable decrease in the pollutants dissolved in the groundwater near B3 was observed when the nitrate solution was used. A full-scale measure was conducted in 2017, with nitrate infiltration occurring from March 28 to October 5, 2017.Groundwater monitoring points B3, B4, B11, and B12 were used as infiltration points. A reduction in pollutants, particularly benzene, was observed near the nitrate input measuring points (B3, B4, B11, B12). However, no reduction in pollutants was observed in the downstream monitoring points (B5, B13) during the seven-month observation period (March to October 2017).

In early October 2019, highly absorbent colloidal activated carbon was introduced into groundwater monitoring points B6, B7, B8, and B10, located along the southwestern boundary of the property. A total of 800 kg of activated carbon CAC was injected into these points using packers. The injection

involved a suspension with a total volume of 80 m^3, containing a concentration of 10 kg/m^3 of activated carbon. The infiltration process was planned to take approximately 40 hours.

The goal was to establish an activated carbon adsorption zone approximately 25 meters wide and 8 meters deep within the groundwater-saturated area, without significantly impacting the hydraulic conductivity of the aquifer.

In December 2020, a combined mechanical and chemical development of monitoring point B7 was conducted as part of the ongoing monitoring.

The following *figure* shows the progression of BTEX concentrations at the infiltration and monitoring points after the colloidal activated carbon infiltration, compared to the concentrations previously recorded at these points.

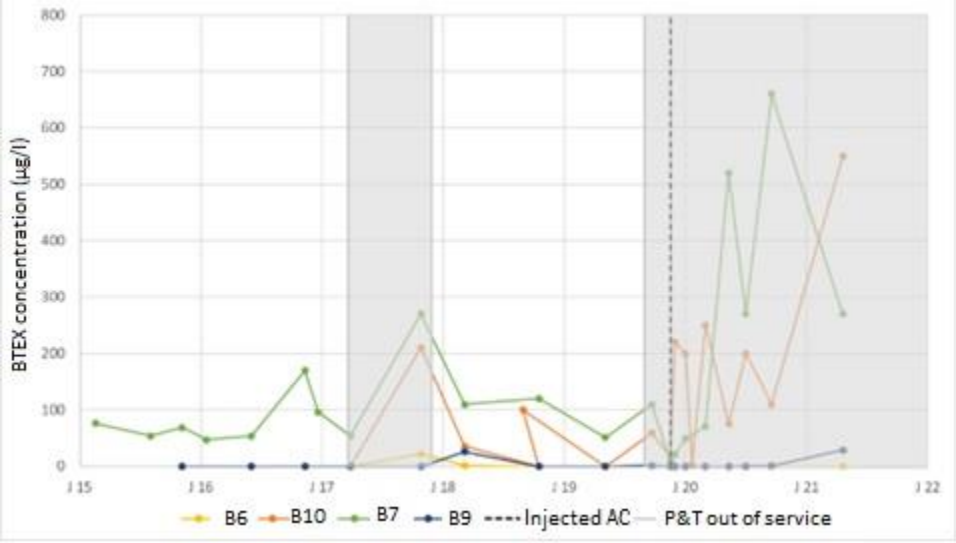

figure 3.5. Concentration development of the infiltration (B6, B7, B10) and downstream monitoring point(s) (B9) before and after the infiltration of the colloidal activated carbon (Arcadis Report)

As illustrated, the dissolved BTEX concentrations at the infiltration points B7 and B10 increased after the colloidal activated carbon was introduced. In B10, the rise in concentration occurred immediately after the infiltration, whereas in B7, it was delayed by approximately 4 months. At the

downstream monitoring point B9, BTEX concentrations also rose about 17 months after the infiltration (April 2021).

This indicates that colloidal activated carbon infiltration was substantially ineffective in preventing the release of pollutants from the source area. Potential reasons for this ineffectiveness could include the uneven formation of the adsorption zone, insufficient concentration of the activated carbon suspension, or the activated carbon's inadequate sorption capacity.

3.7. Conceptual Site Model

The available site data has been compiled into a conceptual site model.

Current groundwater contamination levels include up to 3,790 µg/l of BTEX (B3, April 21, 2021) and up to 1,400 µg/l of TPH (C10-C40) (B5, September 23, 2019). An oil phase with a thickness of up to 1 cm is present at four measuring points (D1, B5, B7, and B13), and in the past, oil phase thicknesses of up to 0.3 m were recorded at certain monitoring points.

The exact pollutant source zones are not known. However, the different BTEX compound compositions observed across the monitoring points suggest at least two main source areas. One is the filling station area, associated with measuring points B3 and B5, and the other is the platform with decommissioned tank containers, linked to measuring point B4. In the filling station area, benzene constitutes more than 95% of the total BTEX, while in the decommissioned tank area, benzene accounts for a lower proportion, mostly 85% or less.

Due to the lower density of LNAPLs compared to water, the groundwater table serves as a barrier to LNAPL migration, with LNAPLs typically accumulating at the interface between the saturated and unsaturated zones.

Changes in the groundwater table, caused by natural fluctuations or human activities, cause periodic displacement of LNAPLs, exposing the soil matrix alternately to saturated and unsaturated conditions, leading to the formation of a "pancake" layer where the LNAPL spreads across the interface between the saturated and unsaturated zones.

As the groundwater table rises and falls, pollutants from the LNAPL migrate into the soil matrix, where they are adsorbed onto soil particles or retained as isolated droplets within pore spaces.

These droplets, often isolated in pore spaces, can remain in the subsurface for long periods, acting as a source of ongoing contamination. This interaction between water (the wetting fluid) and LNAPL (the non-wetting fluid) significantly impacts contaminant transport, retention, and the effectiveness of remediation strategies.

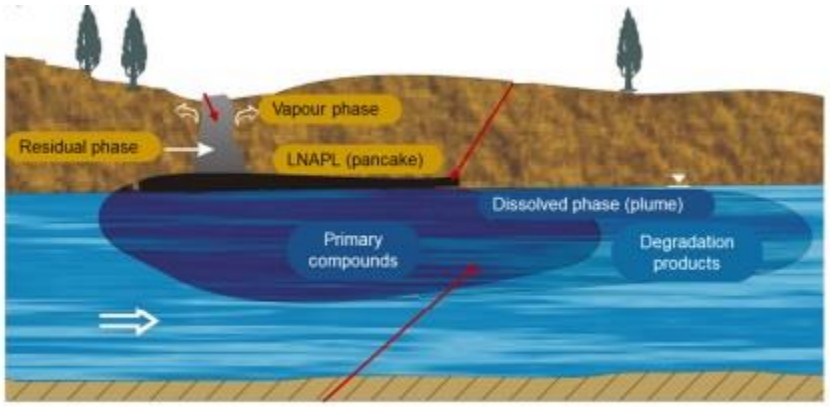

figure 3.6. Dynamics of LNAPL (Groundwater Engineering course notes, Tosco, 2023)

From these areas, as well as from the connected product phase floating on the groundwater, BTEX continue to dissolve into the groundwater, causing persistent contamination of the aquifer.

The groundwater flow direction is southwest to west, towards a river, as confirmed by the orientation of the pollutant plume. The pollutant plume is confined by monitoring points B6, B8, and B9, located at the southwestern edge of the property, where pollutant concentrations are either absent or very low. Inflow into the plume is identified at points B11 and B12, which also show little to no contamination. However, there is no clear delineation of the central portion of the plume in the north-south direction.

The pollutants sustaining the current plume are primarily sorbed to the soil matrix. There is a minor ongoing release of pollutant phase from residual contamination distributed in the pore space, as well as the formation of localized floating oil phase bodies. These residual phase areas continue to contribute to the long-term release of pollutants into groundwater. The slow release of contaminants from low-permeability layers, especially in the predominantly fine-grained aquifer material with silt and gravel layers, is the key factor limiting the remediation timeline. Benzene, which has the highest

eco- and human-toxicological potential, remains the dominant BTEX compound, making up more than 85% of the total.

4. Laboratory Tests

4.1. Methods

Different tests were conducted in the laboratory at Politecnico di Torino to identify the CAC characteristics such as particle size distribution, particle's stability, CAC mobility in the porous medium and, the factors that affect them. The following sections detail the procedures and present the results obtained from these experiments.

4.1.1. Scanning electron microscope (SEM)

Scanning electron microscope (SEM) is one of the most widely used instrumental methods for the examination and analysis of micro- and nanoparticles imaging characterization of objects. One of the reasons that SEM is often preferred over other methods for particle size analysis is due to its resolution of 10 nm. Advanced versions of these instruments can achieve a resolution of about 2.5 nm. (Goldstein, 2012, Raval et al. 2019). The electron beam in an SEM scans the surface of a sample point by point, producing a detailed, two-dimensional image of the sample's topography. We employed this instrument at the Politecnico di Torino laboratory to examine the particle size of CAC, the colloidal activated carbon used for our remediation objective. Four samples, each containing 50 mg/l of CAC, were tested. Since samples must be electrically conductive or coated to prevent charging under the electron beam, a gold coating was used for this purpose.

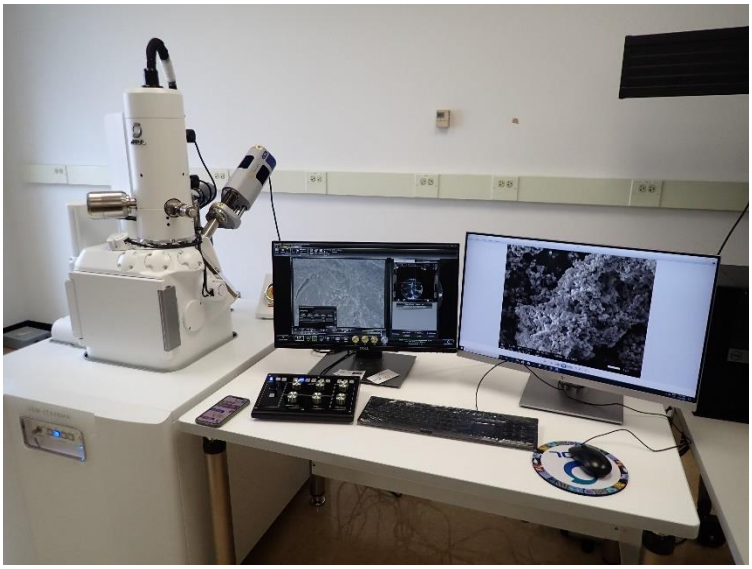

figure 4.1. Scanning electron microscope (SEM), Inspect S, FEI Company, Hillsboro US ("Scanning Electron Microscopy," n.d.)

4.1.2. Energy Dispersive X-ray

In the context of Scanning Electron Microscopy (SEM), it is an analytical technique used to determine the elemental composition of a sample. It involves detecting X-rays emitted from the sample when it is bombarded with an electron beam in the SEM (Hellmy and Azida 2023), (Mishra, Zachariah, and Thomas 2017).

4.1.3. CPS disc centrifuge

The CPS disc centrifuge analyzes particle size distributions through centrifugal sedimentation. In this process, particles settle in a fluid under centrifugal force, with their sedimentation speed depending on their size and density. The sample is injected at the center of the rotating disc, where all particles begin sedimenting simultaneously. The sedimentation velocity increases with the square of the particle diameter, so even small differences in particle size led to noticeably different settling rates, with larger particles settling faster. This makes centrifugal sedimentation ideal for high-resolution particle size analysis.

To overcome the slower settling rates of small, low-density particles, the CPS centrifuge applies extremely high rotational speeds. As the disc spins at high speeds, centrifugal force drives the

particles outward toward the edge. Particles of the same size settle at the same speed, forming distinct, thin bands that reach the detector together. Larger particles arrive at the detector earlier than smaller ones, while particles with closely similar sizes are detected at slightly different times, allowing for precise differentiation.

At the disc's outer edge, a 405 nm light beam detects particles as they pass through, absorbing light in proportion to their presence. The time it takes for particles to sediment from the center to the detector, combined with light absorption data, is used to calculate particle size distribution. This process is based on Stokes' Law for sedimentation and Mie Theory for light diffraction. The disc's high rotational speed accelerates the analysis, enabling even very small and lightweight particles to be measured accurately within a short timeframe (Quantum Design, Italy, Instrument manual).

figure 4.2. CPS disc centrifuge, Oosterhout RC ("Products," n.d.)

For this thesis, we injected a 1 g/l solution of CAC, diluted with deionized water (DIW), into the instrument and monitored the results. The test required approximately 2 hours and 30 minutes to complete.

4.1.4. dynamic light scattering (DLS)

The Zetasizer Nano range of instruments enables the measurement of three key properties of particles or molecules in a liquid medium: particle size, zeta potential, and molecular weight. (Malvern Instruments Zetasizer Nano Series User Manual, Feb. 2004).

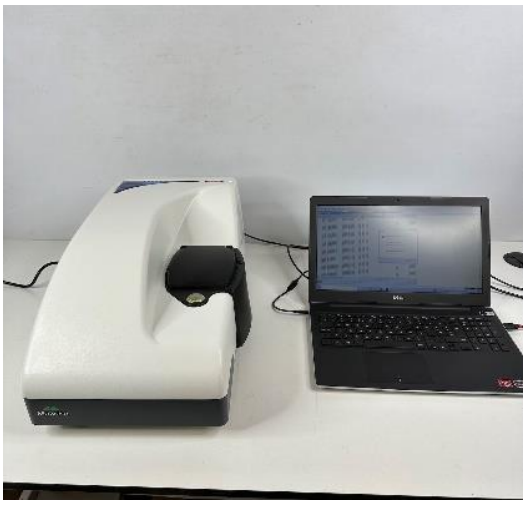

figure 4.3. Zetasizer nano, Malvern Panalytical, Malvern UK ("Malvern Zetasizer Nano ZS ZEN3600 Size and Zeta Potential Particle Size +PC, S/W - SOLD," n.d.)

Particle size refers to the diameter of a sphere that diffuses at the same rate as the particle being measured. The Zetasizer system determines particle size by measuring the Brownian motion of particles in a sample through dynamic light scattering (DLS) and then applying established theories to interpret the size. In a liquid, particles exhibit random motion, and their speed of movement is directly related to their size—smaller particles move faster, while larger particles move more slowly. By taking two measurements of the sample over a short time interval, such as 100 µs, the distance the particles have moved can be observed. If the particles have moved very little, the sample contains larger particles; if they have moved significantly, the sample contains smaller particles (Malvern Instruments Zetasizer Nano Series User Manual, Feb. 2004).

Most liquids contain ions, which can be either positively charged (cations) or negatively charged (anions). When a charged particle is suspended in a liquid, ions of the opposite charge are attracted to the surface of the particle. For instance, a negatively charged particle attracts positive ions from the liquid, and a positively charged particle attracts negative ions. The ions closest to the particle

surface are strongly bound, while those farther away are loosely attached, forming a diffuse layer. Within this layer is a notional boundary called the slipping plane. Ions within this boundary move with the particle when it moves through the liquid, while ions outside the boundary remain in place (Malvern Instruments Zetasizer Nano Series User Manual, Feb. 2004).

The Zeta potential refers to the potential difference between the particle surface and the dispersing liquid at the slipping plane. The layer typically referred to as the slipping plane serves as the boundary between strongly bound ions and bulk solutions. (Fedele et al. 2011) ("Zeta Potential," n.d.). The zeta potential indicates whether particles in a liquid will tend to flocculate (clump together) or remain dispersed.

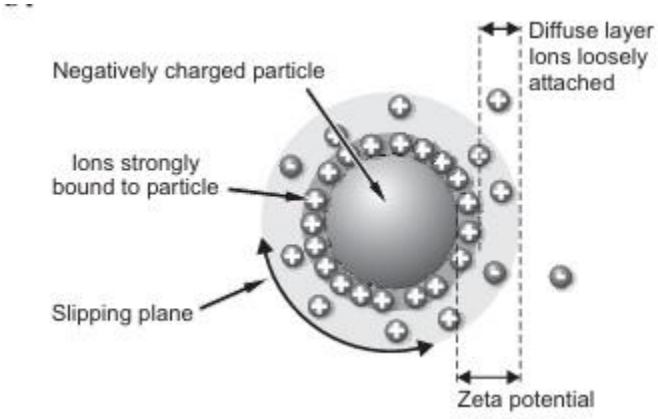

figure 4.4. Electrical double layer and zeta potential around a charged particle (Malvern Instruments Zetasizer Nano Series User Manual, Feb. 2004)

Zeta potential is essential for understanding the stability of colloidal systems. A higher zeta potential (between ±15 mV and ±30 mV, depending on the specific system, such as the ionic strength of the medium, particle surface chemistry, and etc.) generally indicates greater stability, as particles with a high zeta potential push back one another, reducing the likelihood of aggregation. This repulsion helps to keep the particles dispersed and prevents them from clumping together (Malvern Instruments Zetasizer Nano Series User Manual, Feb. 2004).

The other parameter, The zeta average refers to a mean hydrodynamic diameter of particles in a sample. ("What Is the Z-Average? | Malvern Panalytical," n.d.) (Bhattacharjee 2016).

When a sample contains particles of various sizes, the DLS analysis often displays multiple peaks, each representing a different population of particles.

Peak 1 (often indicated as Pk 1) is the most abundant peak in the size distribution. The mean size associated with peak 1 (PK 1 mean) is an important value because it provides the average size of the most abundant particles.

Pk 1 mean helps assess the stability of the smallest particles. A significant shift in Pk 1 mean overtime can indicate changes like aggregation or degradation.

In our laboratory tests, once the optimal dilution of CAC (1 g/l) was determined for continuing the laboratory tests, NaCl in various concentrations (1mMol,3mMol,5mMol,10mMol,30mMol,50mMol,100mMol) was added to colloidal activated carbon to study how ionic strength affects controlling zeta potential, colloidal stability and aggregation.

4.1.5. Ultraviolet–visible (UV–Vis) absorption spectroscopy

UV-Vis spectroscopy is an analytical method used to quantify the absorption or transmission of ultraviolet (UV) and visible (Vis) light by a sample across a wavelength range, typically between 190 and 900 nm. This method is based on the interaction of light with matter, where molecules in the sample absorb light at the specific wavelengths. The spectrophotometer measures the intensity of light transmitted through the sample and compares it to the intensity transmitted through a reference or blank, which contains only the solvent or matrix without the analyte of interest. The resulting data is expressed as absorbance, which is proportional to the concentration of the absorbing species (“UV-Vis Spectroscopy: Principle, Strengths and Limitations and Applications,” n.d.).

Light possesses a specific amount of energy that is inversely related to its wavelength; shorter wavelengths correspond to higher energy, while longer wavelengths carry less energy. For electrons in a substance to be excited to a higher energy state, a precise amount of energy is required, which we observe as light absorption. The energy needed to promote electrons varies depending on their bonding environment within a substance. This difference in required energy explains why different

substances absorb light at distinct wavelengths (“UV-Vis Spectroscopy: Principle, Strengths and Limitations and Applications,” n.d.) (Chen et al. 2025) (Pilaquinga et al. 2024).

It is possible to determine the chemical or physical properties of the sample too. In general, it is possible to:

- Identify molecules in a solid or liquid sample
- Determine the concentration of a particular molecule in solution
- Characterize the absorbance or transmittance through a liquid or solid over a range of wavelengths
- Characterize the reflectance properties of a surface or measuring the color of a material
- Study chemical reactions or biological processes

(Agilent, The Basics of UV-Vis Spectrophotometry, A primer)

figure 4.5. Spectrophotometer Specord S600, Analytik Jena, Jena - Germany

For this thesis, sedimentation tests were carried out using this instrument to measure the changes in the concentration of suspended particles of CAC over time. The tests were conducted with preparing the samples of the 0.5 g/l,0.75 g/l and 1 g/l of CAC in DIW, as well as for the 1g/l of CAC + different mMol NaCl concentrations. We should ensure that the sample suspension is well-mixed before putting it into the instrument to achieve uniform particle distribution. After reaching the result

of the tests, we normalized the concentration with having the initial concentration and the concentration at each time point (C/C_0). This step standardizes the results and provides a dimensionless value for easy comparison. By plotting (C/C_0) against time, we will have the sedimentation curve that shows the decline in particle concentration as sedimentation progresses.

The calibration curve, used to determine the concentration of an unknown substance by comparing it to a set of reference samples with known concentrations. By analyzing the relationship between concentration and the instrument's response, the curve can predict unknown concentrations and establish detection and quantitation limits. (Ken Philips, 2024) (Inga Pacharzina, 2022).

4.1.6. Column tests

Column tests can be sometimes used to assess the efficacy of sorbing materials, such as activated carbon (AC) and anion exchange resins (AER) in removing contaminants from impacted waters. Column tests allow for enhanced mass transfer and simulation of long-term field or pilot testing in a much shorter time frame under controlled laboratory settings (Nguyen and Schaefer 2023).

To achieve our target for this thesis, we first prepared the column. A vertical column with a diameter of 1.8 cm and a length of 10 cm was filled with 37 g of pre-washed sand using deionized water (DIW). Both ends of the column were sealed, and it was saturated with water to simulate real field conditions. Inlet and outlet tubes were connected to the column for injection and for collecting samples after the solution passed through the column.

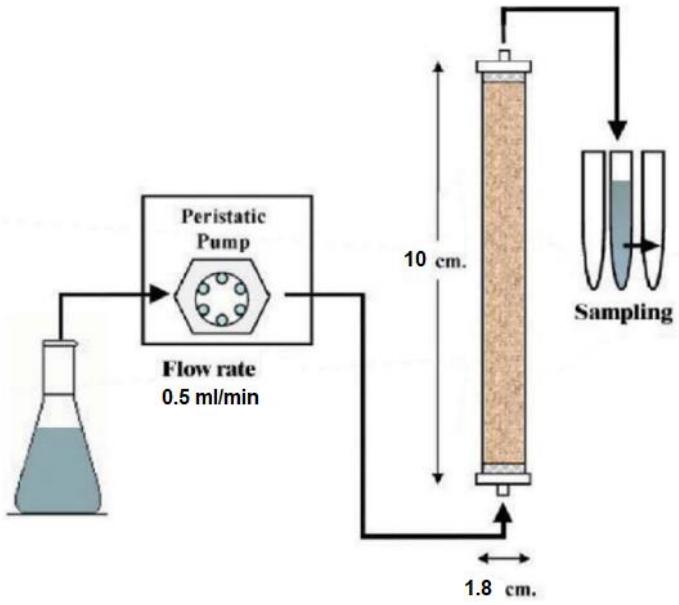

figure 4.6. Column test setup (Eslami et al. 2017)

It was also essential to calculate the velocity at which groundwater moves through the column, as an excessively fast flow would reduce the contact time between the contaminants and the treatment medium, potentially compromising remediation efficiency. We began the test by injecting deionized water (DIW) into the column with a peristaltic pump (Peristaltic pump Imsatec Reglo Pump, Ismatec, Glattbrugg, Switzerland) to clean and equilibrate it with a flow rate (Q) of 0.5 ml/min:

$$A = \pi r^2 = 3.14 * (0.9)^2 = 2.54 \ cm^2$$

$$V = \frac{Q}{A} = \frac{0.5}{2.54} = 0.196 \ {}^{cm}/_{min}$$

The optimal pump pulse determined as 0.820 ml/min.

After an initial period, DIW was replaced by a 30 mMol NaCl solution used as a tracer. Injecting NaCl as a nonreactive tracer was to determine the effective porosity and dispersivity of the column which are essential for understanding solute and particle mobility.

The tracer front becomes dispersed along the flow path, with the extent of spreading increasing as the travel distance grows. This dispersion occurs because kinematic dispersion cause some tracer molecules to move at speeds greater than, and others slower than, the average velocity of water (R.Allan Freeze, n.d).

As we calculated the Darcy velocity before, having the flow rate (Q) and cross sectional (A), we can calculate the effective porosity (n_e) as below:

$$n_e = \frac{Q}{A.V} = \frac{0.5}{2.54 * 0.196} = 1.02$$

Following the NaCl injection, a 1 g/l dilution of CAC suspension was injected at the same rate. The outflow concentration was measured in-line and continuously using flow-through cells connected to a spectrophotometer. The flow-through cells were equipped with an inlet tube and an outlet tube. One flow-through cell was not connected to the column allowing for the direct measurement of the input concentration, while another was connected to the column outlet enabling the measurement of the outlet concentration over time. This setup allowed for an accurate comparison between the input and output concentrations. Outflow samples were collected from every 17 minutes during the test.

The spectrophotometer measured the absorbance of the outflow samples which is directly proportional to the concentration of the CAC suspension. In this case, absorbance was normalized (A/A_0) to simplify the analysis and have the breakthrough curve.

The CAC concentration in the column is often expressed as relative concentration, defined as C/C_0, where C represents the concentration within the column or at the outlet, and C_0 is the initial input concentration. This allows the CAC input to be modeled as a step function for simplicity. The relationship between concentration and time at the column's outlet is referred to as the breakthrough curve (R.Allan Freeze, n.d.).

The entire test lasted approximately 2 hours and 50 minutes.

4.2. Results

4.2.1. Scanning electron microscope (SEM)

The following figures display two selected SEM images among all 11 images that we obtained for the particle size of CAC within the samples.

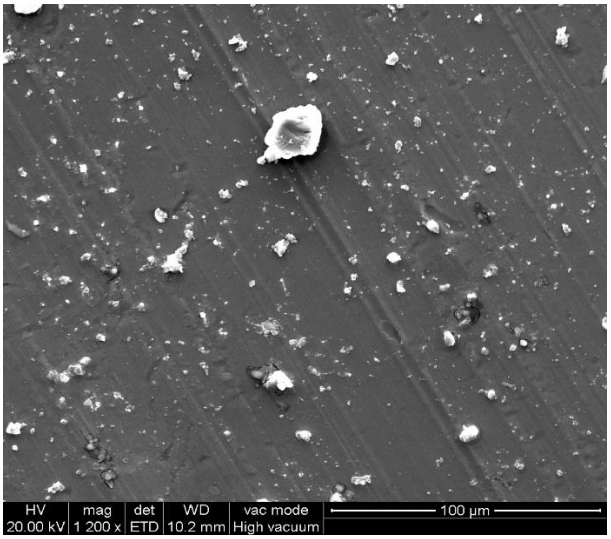

figure 4.7. CAC *particle size from SEM*

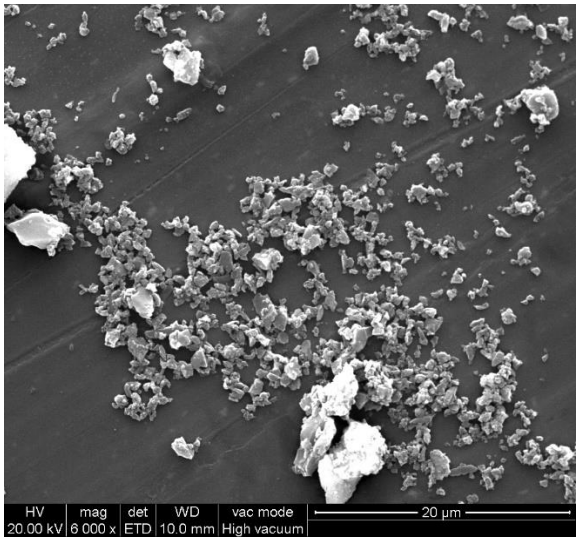

figure 4.8. CAC *particle size from SEM*

Based on the images and size scales indicated on each image, *Table 4.1* has been created to present a classification of particle size of CAC samples used for this test, categorized into four different ranges. It shows the particle size distribution of samples in each class by percentage.

	Lower than 1 µm	**1-5 µm**	**5-10 µm**	**10-20 µm**
Sample 1	58.63	34.13	3.61	3.61
Sample 2	53.61	37.34	7.22	1.80
Sample 3	43.33	25	13.33	18.33

Table 4.1. Particles size classification (%)

Most of the particles in the images fall into the smallest size range (lower than 1 µm). This indicates that the samples are primarily composed of small particles, which are consistent with the behavior of colloidal materials that typically have very fine particles.

The second most frequent size range is 1-5 µm. This suggests a relatively balanced particle size distribution within this range for some samples.

As the particle size increases, the number of particles decreases significantly. This distribution shows that large particles are relatively scarce across all samples, and the material is primarily composed of smaller particles.

The predominance of small particles (lower than 1 µm) across most samples is beneficial for groundwater remediation, as smaller particles have a larger surface area-to-volume ratio ("Exchange Surfaces - Surface Areas to Volume Ratios (GCSE Biology)," n.d.). This allows for more efficient adsorption of contaminants like BTEX or other pollutants.

Figure 4.9 shows a graphical comparison of the four particles size classes for the CAC samples based on *Table 4.1*.

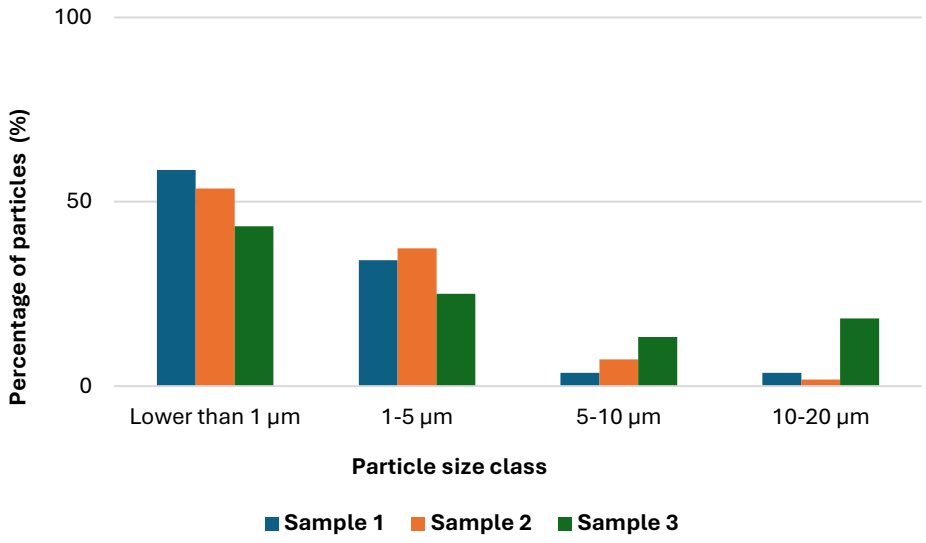

figure 4.9. Comparison of particle size distribution among CAC samples (%)

We generally expect CAC samples to have approximately the same particle size distributions in case they are from the same source and prepared from the same batch of CAC. However, differences

arise because CAC is a heterogeneous material, made up of irregularly shaped particles with a range of sizes. So, different samples may experience local variations during handling, dispersion, or sampling from different parts of a batch.

Moreover, in the process of preparing samples for SEM imaging, differences in dispersion technique can lead to differing levels of aggregation, resulting in varying distributions.

Also, in SEM analysis, the images may only represent a small portion of the sample. If areas with more or fewer fine particles are selected, it can skew the observed size distribution.

4.2.2. Energy Dispersive X-ray

As we can see in the figures below, most samples have a high carbon content, indicating the presence of carbon-based materials or organics. Aluminum is the coating metal of the tapes. Also, silicon, sodium, potassium, and magnesium were detected in several samples. Some samples contain gold, due to the coating process used in sample preparation for SEM analysis.

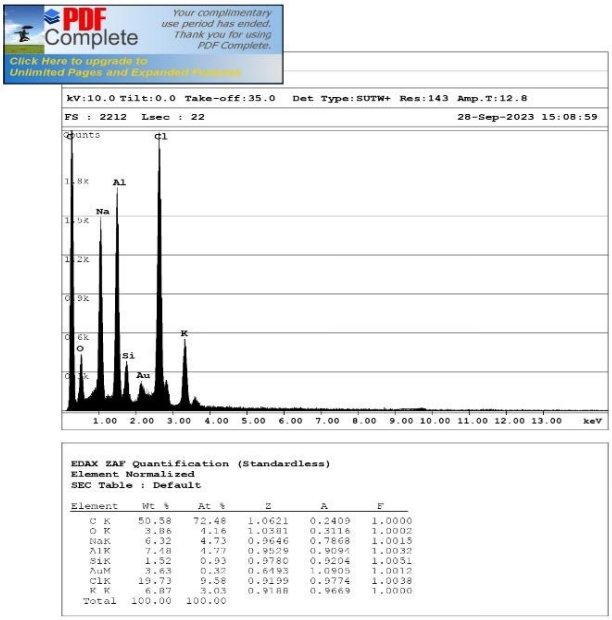

figure 4.10. EDX-Ray quantification

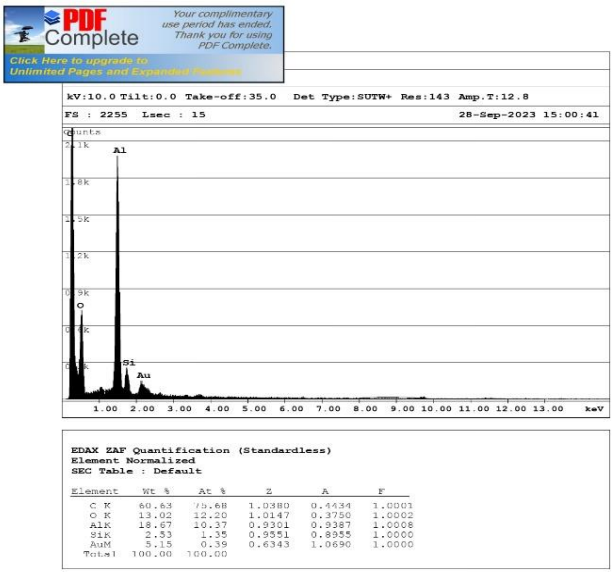

figure 4.11. EDX-Ray quantification

4.2.3. CPS Disc Centrifuge

Figure 4.12 shows the size and cumulative distribution in mass.

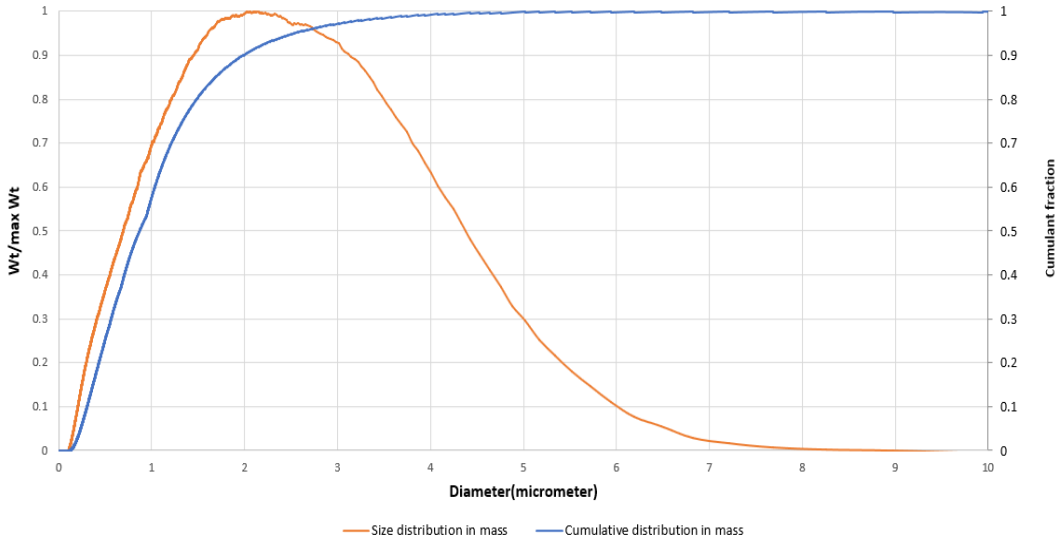

figure 4.12. Particle distribution in mass

The orange line shows the size distribution in mass. This curve represents the mass distribution of the particles. The y-axis indicates the relative mass of particles for each particle diameter, while the x-axis shows the particle diameter.

The peak of the curve occurs around 2.2 µm, indicating that the majority of the particle mass is concentrated around this size.

The mass distribution curve tails off as the particle size increases, showing that particles larger than 3 µm are less prevalent. Beyond 6 µm, the contribution to mass becomes negligible.

The blue line shows the cumulative distribution in mass. This line shows the cumulative fraction of mass for particles smaller than a given diameter. The representative sizes of cumulative distribution are:

d_{10} = 0.3 µm

d_{50} = 0.85 µm

d_{90} = 2.016 µm

Figure 4.13 shows the size and cumulative distribution in number.

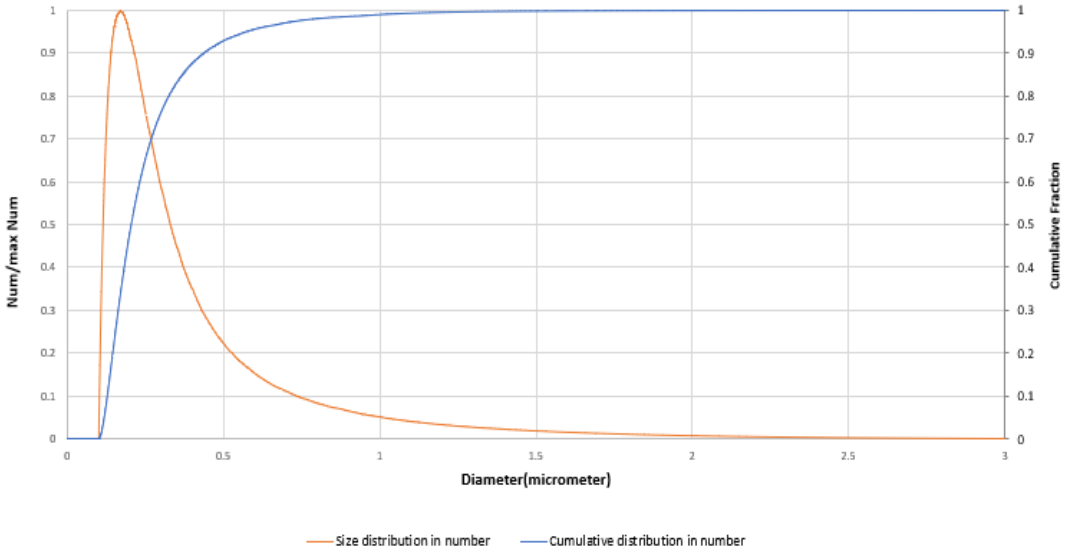

figure 4.13. Particle distribution in number

The orange line shows the size distribution in number. This line shows the distribution of particles by their size, with the x-axis representing particle diameter (in micrometers, µm) and the y-axis representing the relative number of particles of each size.

It indicates that the majority of the particles are concentrated at smaller diameters, with a peak around 0.12 µm, after which the number of particles sharply decreases as the particle diameter increases.

The particle size distribution is highly skewed towards smaller particles, with most of the particles falling below 0.5 µm.

The blue line shows the cumulative distribution in number. This line represents the cumulative percentage of particles below a certain diameter. As the curve rises, it shows the proportion of particles that are smaller than a given size.

At d_{50} = 0.202 µm, 50% of the particles are smaller than this diameter, indicating the median particle size. Similarly d_{10} = 0.12 µm and d_{90} = 0.43 µm.

The cumulative curve flattens after about 1 µm, indicating very few particles are larger than this size.

4.2.4. Dynamic Light Scattering (DLS)

Figure 4.14 shows the relationship between CAC concentration and the Z-average particle diameter (measured in nanometers, nm). The Z-average, as explained earlier, is an intensity-weighted mean particle size that provides insight into how the particles behave in suspension.

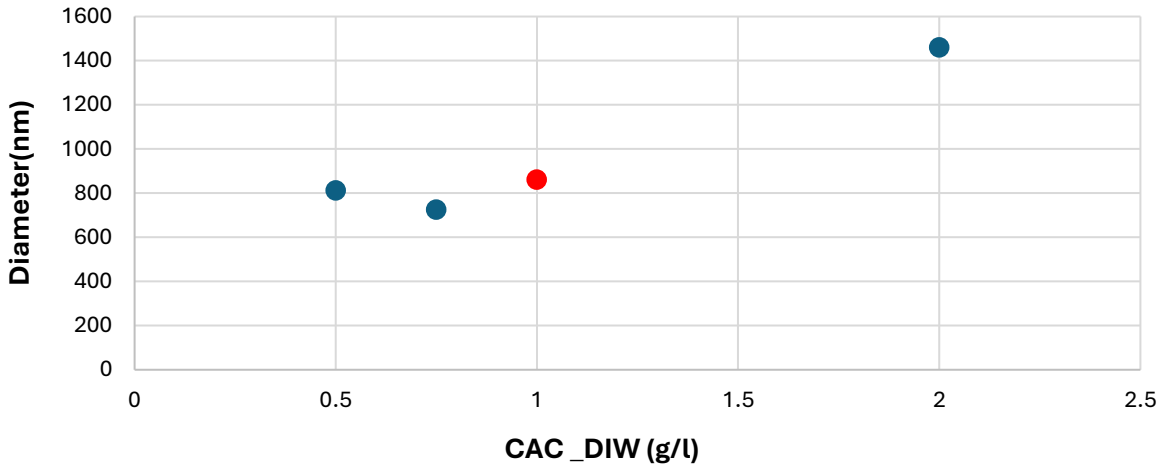

figure 4.14. Z-average particle diameter of CAC, different concentrations in DIW

The concentration of CAC in deionized water (DIW) ranges from 0.5 to about 2.0 g/l. Meanwhile The Z-average diameter of particles ranges from about 700 nm to slightly 1500 nm.

At low concentrations (0.5 to 1 g/l), the particle size remains relatively constant, fluctuating around 800 to 1000 nm. This suggests that in this concentration range, the particles are well-dispersed, and the Z-average size does not significantly change as the concentration increases. The CAC particles maintain good colloidal stability, with minimal aggregation.

At higher concentration (2 g/l), the Z-average diameter increases significantly, reaching nearly 1500 nm. This could indicate particle aggregation at higher concentrations, where particles tend to cluster together.

Figure 4.15 shows the Pk 1 mean CAC (the mean size of particles in the first peak, based on intensity) as a function of the CAC concentration in deionized water (DIW).

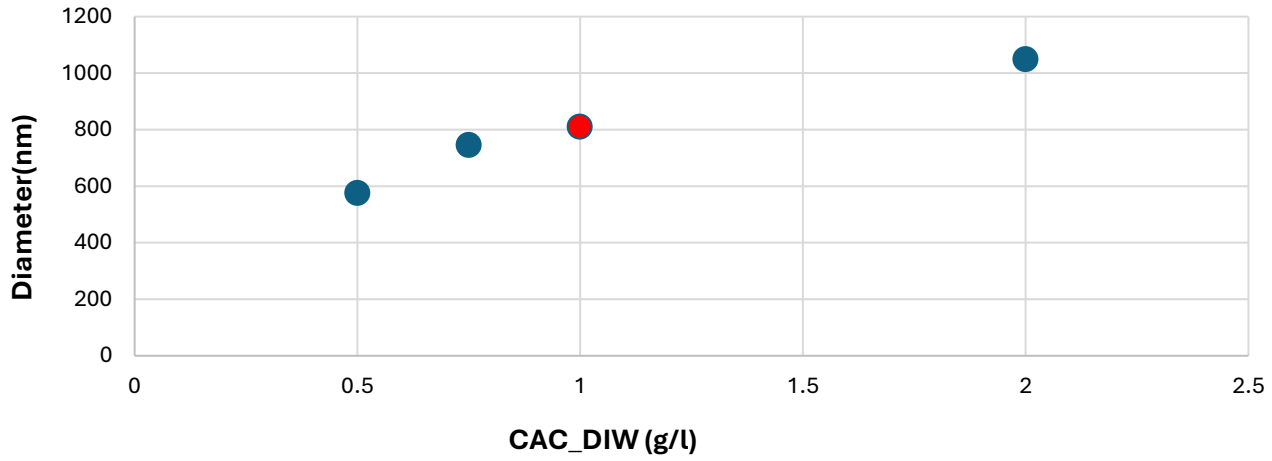

figure 4.15. Pk 1 Mean CAC, different concentrations in DIW

The Pk 1 mean CAC ranges between 600 nm to about 1100 nm.

As the concentration of CAC increases from 0.5 g/l to 2 g/l, the particle size in the first peak gradually increases from around 600 nm to just above 1000 nm.

In the lower concentrations (0.5 - 1 g/l), the particle sizes remain relatively stable, with only a small increase in the mean size from about 600 nm to 850 nm.

In the higher concentration (2 g/l), the particle size shows a significant increase to around 1100 nm, suggesting potential aggregation or changes in particle behavior at higher concentrations.

The graph suggests that as the concentration of CAC increases, the size of the smallest particles (Pk 1 mean) gradually increases, particularly at concentrations above 1 g/l. This could indicate that at higher concentrations, particles tend to aggregate or form larger clusters, which leads to an increase in the mean particle size.

Figure 4.16 reports two graphs from the dynamic light scattering (DLS) analysis for dilution of 1 g/l of CAC, which shows the raw correlation data and the size distribution by intensity of the sample.

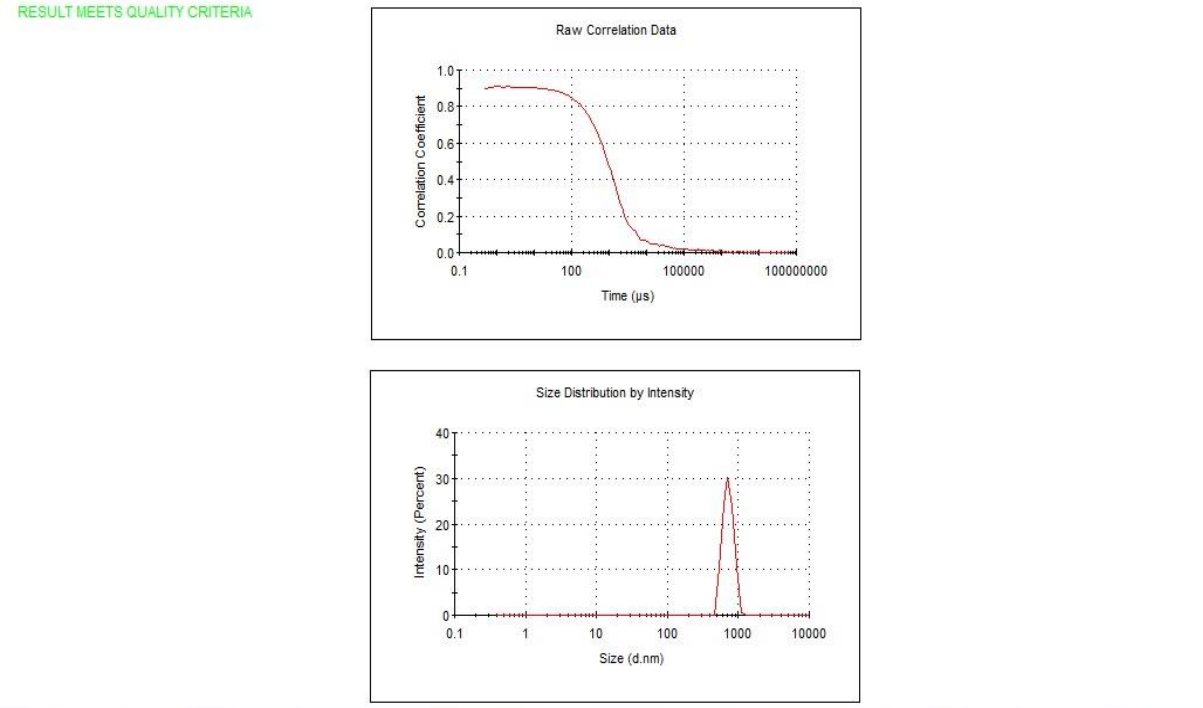

figure 4.16. raw correlation data and the size distribution of CAC 1g/l

Raw Correlation Data (Top Graph)

The x-axis represents time in microseconds (µs), and the y-axis represents the correlation coefficient. This correlation is used to determine the size of particles in the sample by analyzing how the scattered light changes over time.

This graph shows how the light scattered by the particles in the sample loses correlation over time. Larger particles tend to diffuse more slowly, resulting in a slower drop in the correlation coefficient, while smaller particles diffuse faster, leading to a quicker drop-off.

The rapid decrease in the correlation coefficient at around 100,000 µs suggests the presence of relatively large particles or particle aggregates (much possible according to the other test results) in the sample. This is because larger particles cause a more sustained correlation signal.

Size Distribution by Intensity (Bottom Graph)

The x-axis represents particle size (in nanometers, nm), while the y-axis represents the intensity (%) of the scattered light.

The peak in intensity is located around 1000 nm, meaning that most of the particles in the sample have a size around 1000 nm. There are no significant secondary peaks, indicating that the sample is relatively monodisperse.

Based on the results, we have determined that 1 g/l is the optimal dilution for the CAC suspension.

Figure 4.17 shows zeta average measurement for the best CAC dilution (1 g/l) with addition of NaCl.

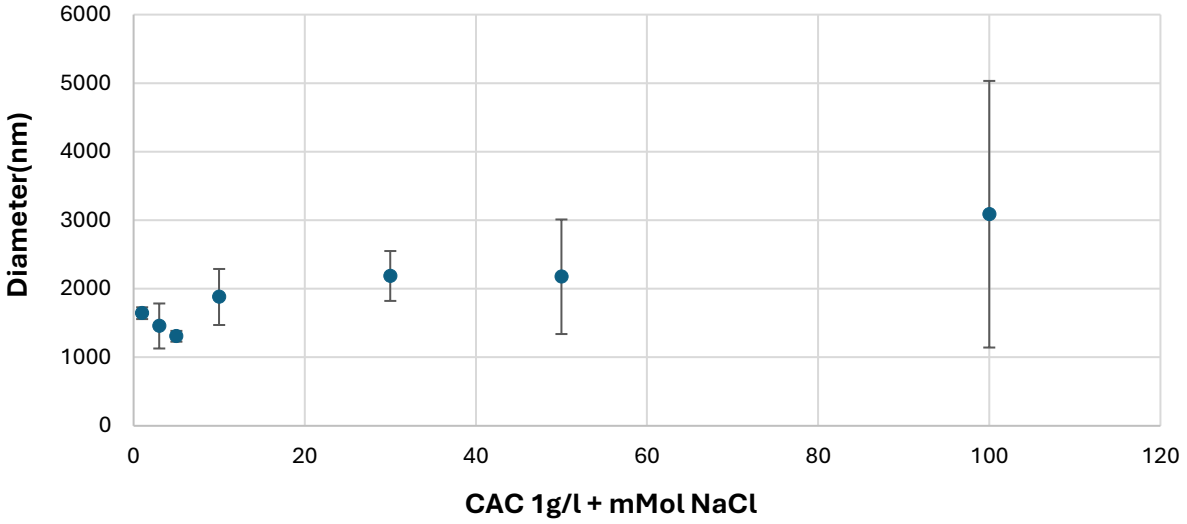

figure 4.17. Zeta average CAC1g/l + mMol NaCl

The Y-axis represents the diameter (nm), and the X-axis reports the molar concentration of NaCl added to the CAC suspension at 1 g/l. The data points are accompanied by error bars.

The diameters slightly increase with increasing NaCl concentration. The values start from just over 1800 nm at 0 mMol NaCl and continue rising towards 3000 nm around 100 mMol NaCl.

At lower concentrations of NaCl (0-20 mMol), the standard deviation is relatively small, suggesting that the measurements are consistent and precise. The particle diameters show minor variations.

As the NaCl concentration increases, particularly near 50 and 100 mMol, the standard deviation significantly increases, indicating greater variability in the particle size distribution at higher salt concentrations.

Figure 4.18 shows the Pk 1 mean NaCl as a function of NaCl concentration. The y-axis represents the diameter of particles (nm), and the x-axis reports the molar concentration of NaCl added to the CAC suspension at 1 g/l.

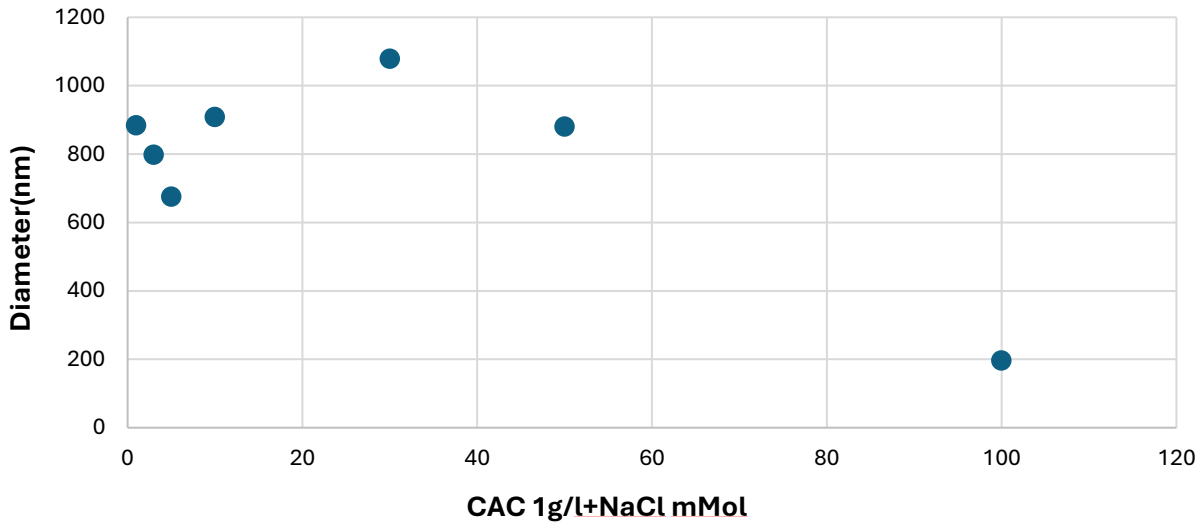

figure 4.18. Pk 1 mean CAC 1 g/l + NaCl mMol

The peak diameter shows oscillating values in the range 0-30 mM NaCl, with values around 800-1000 nm, and decreases for higher NaCl concentrations reaching around 200 nm at 100 mMol NaCl.

This suggests that NaCl induces changes in the particle stability, likely promoting the sedimentation of the larger particles and aggregates, which result in only smaller particles remaining suspended in solutions for higher NaCl concentration. This is in agreement with the observed decrease in the Z-average size increases.

The zeta potential of CAC at a concentration of 1 g/l in deionized water (DIW), the zeta potential varies between -14 mV and -22 mV, with most values closer to -20 mV. For CAC in Tap Water, the Zeta potential is less negative, around -10 mV. Higher magnitude (more negative) zeta potential generally indicates better particle stability, as electrostatic repulsion prevents particles from aggregating. It

indicates that CAC dispersion is more stable in deionized water (DIW) than in tap water, as evidenced by the more negative zeta potential in DIW.

For CAC in DIW, the more negative zeta potential (near -20 mV) suggests relatively better stability compared to tap water. The higher ionic strength of tap water leads to an increased number of ions, which in turn screen the charges on the surface of the particles. This reduces the absolute value of the zeta potential, potentially encouraging phenomena like aggregation.

For CAC in tap water, the zeta potential is closer to -10 mV, indicating lower stability. Tap water does contain ions that shield the charges on the particle surface, reducing electrostatic repulsion and thereby leading to lower zeta potential values.

Figure 4.19 illustrates the zeta potential of CAC (1 g/l) at various concentrations of NaCl (ranging from 1 mM to 100 mM), with the zeta potential (in millivolts) plotted on the y-axis and NaCl concentration (in mM) on the x-axis.

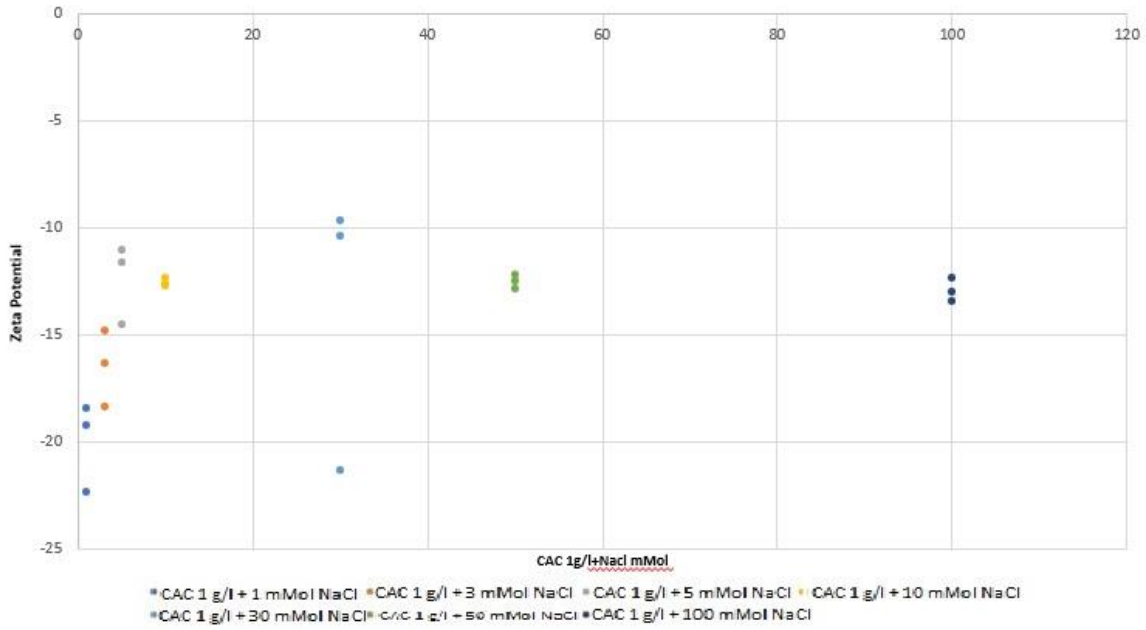

figure 4.19. Zeta potential of CAC 1g/l + different concentrations of NaCl

At lowest NaCl concentration (1 mMol), the zeta potential is close to -20 mV, indicating moderate colloidal stability. With increasing NaCl concentration, the absolute value of the zeta potential

decreases and for NaCl concentrations of 15 mM and above its average value stabilizes approximately at -12 mV, indicating a mildly unstable suspension.

4.2.5. Ultraviolet–visible (UV–Vis) absorption spectroscopy

Figure 4.20 represents the absorption spectra of CAC at three different concentrations (1 g/l, 0.75 g/l, and 0.5 g/l) over a range of wavelengths (λ) from 200 nm to 1100 nm.

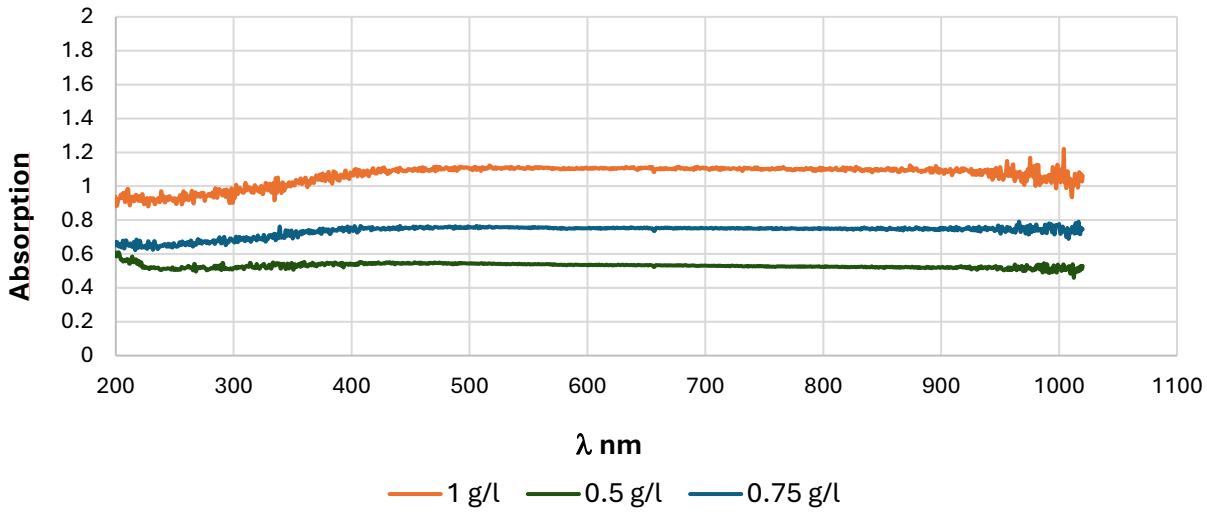

figure 4.20. Absorption spectra of CAC at three different concentrations

The graph shows near-constant absorption across the spectrum from 200 nm to 1100 nm for all three concentrations.

The three concentrations show a consistent pattern of absorbance across this wavelength range with small variations.

As expected, the absorbance increases with higher concentration, the greater the concentration, the higher the absorbance due to more particles or molecules in solution.

Figure 4.21 represents the absorption spectra of CAC 1 g/l + mMol NaCl at different concentrations (ranging from 5 mM to 100 mM) over a range of wavelengths (λ) from 180 nm to 1100 nm.

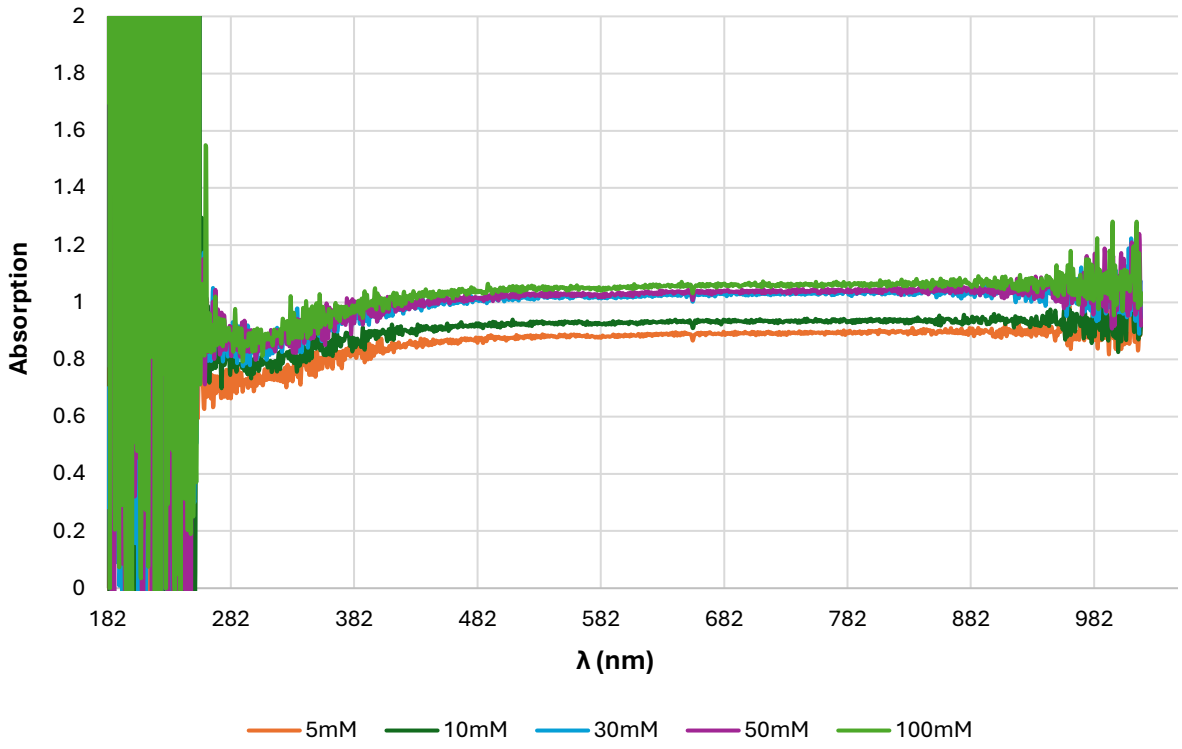

figure 4.21. Absorption spectra of CAC 1 g/l + mMol NaCl at different concentrations

The fluctuations for absorption values below 200 nm indicate instrumental noise. It's common for UV-Vi's spectrophotometers to exhibit noise in the lower UV range when measurements approach the limits of detection for the instrument.

At higher salt concentrations (like 100 mM and 50 mM), the absorption is consistently greater compared to lower concentrations such as 5 mM and 10 mMol. This trend is clearly evident in the 400–900 nm range. The likely explanation is that higher salt levels reduce the electrostatic repulsion between colloidal particles, leading to aggregation. These aggregated particles scatter more light, which results in a higher absorption. Essentially, the increased ionic strength destabilizes the colloidal system, encouraging particle aggregation.

4.2.6. Calibration Curve

Figure 4.22 is the calibration curve at 500 nm wavelength that provides a better linear relationship between absorbance and concentration compared to the ranges below or above that, with the equation of the line displayed as y=1.0709x and a high R^2 value of 0.9985.

The R^2 value of 0.9985 indicates a good fit between the data points and the line meaning the concentration and absorbance are strongly correlated.

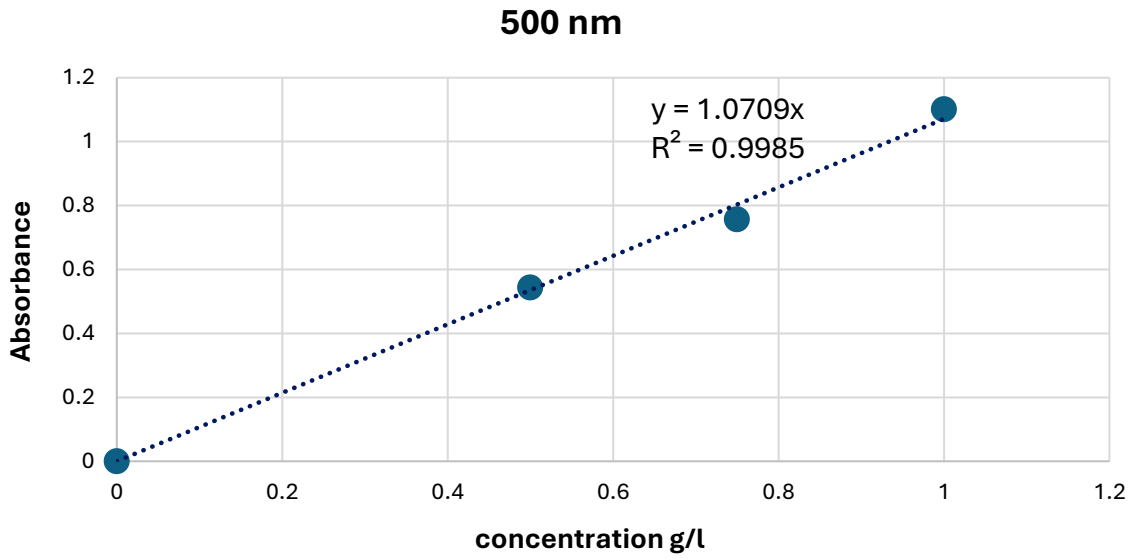

figure 4.22. Calibration curve at 500 nm wavelength

Figure 4.23 shows the results of the sedimentation test over time, with sedimentation (C/C_0) plotted on the y-axis, represents the concentration of particles remaining in suspension at a given time, normalized to the initial concentration C_0, and time (in hours) on the x-axis. The concentration data were derived from the breakthrough curve and normalized to the initial concentration (C/C_0), allowing for a direct comparison of relative concentration changes over time. The different curves (0.75 DIW, 0.5 DIW, and 1 DIW) represent different concentrations of CAC in deionized water (DIW).

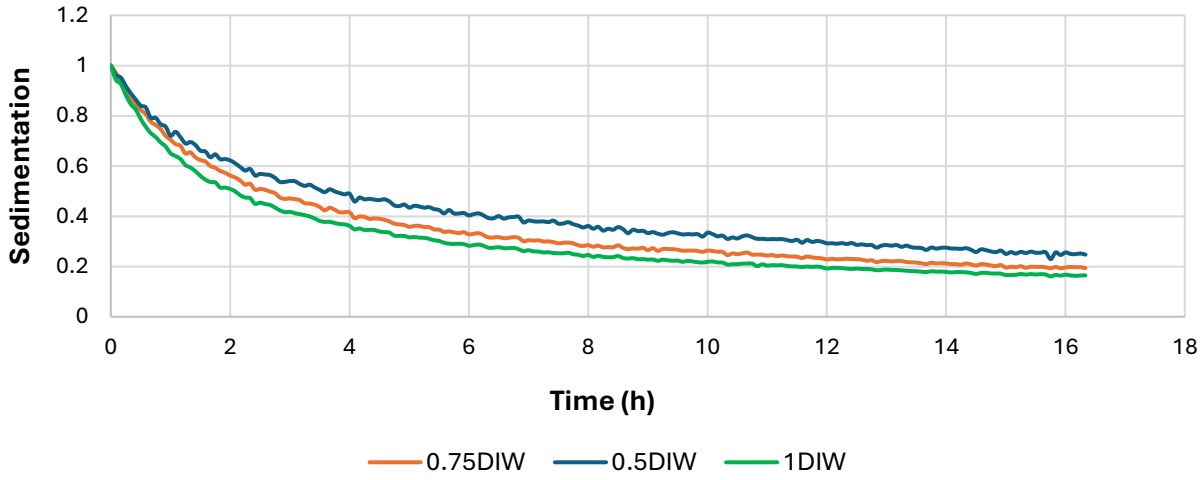

figure 4.23. Sedimentation over time for CAC concentration in DIW

All suspensions show a decreasing trend in sedimentation (C/C_0) over time, indicating that particles are settling out of suspension. The sedimentation rate is higher for the most concentrated suspension (1 g/l) and lower for lower concentrations, indicating that more diluted suspensions are more stable.

The half-time for sedimentation (i.e. the time it takes for the suspension concentration to reach 50% of its initial value, or $C/C_0 = 0.5$) is:

- 1 g/l DIW: 1.9 hours.
- 0.75 g/l DIW: 2.58 hours.
- 0.5 g/l DIW: 3.75 hours.

These values indicate that as the concentration decreases, the time required for the suspension to reach 50% of its initial concentration increases. Lower concentration suspensions take longer to reach the halfway sedimentation point, reflecting faster sedimentation rates in more concentrated samples.

Figure 4.24 shows the half-time ($C/C_0 = 0.5$) in hours for sedimentation of different concentration of CAC (in g/l).

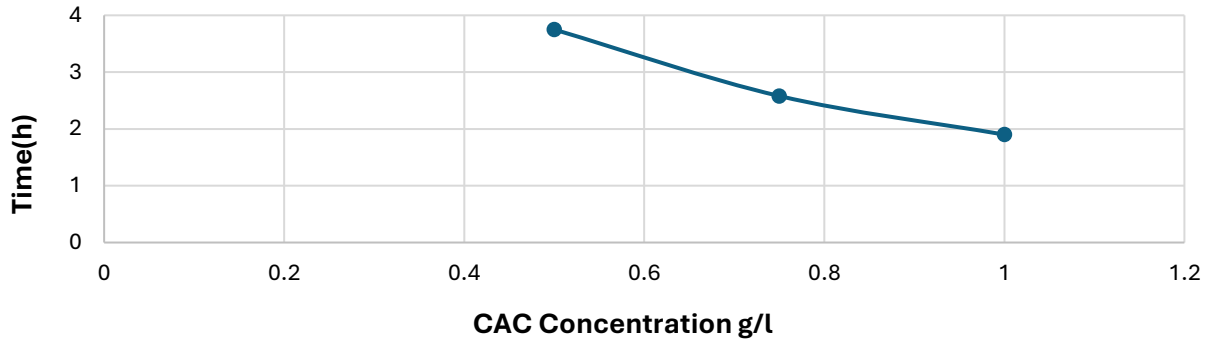

figure 4.24. Half-time for sedimentation of different concentration of CAC

Figure 4.25 shows the results of the sedimentation tests at different concentrations of NaCl (ranging from 1 mM to 100 mM).

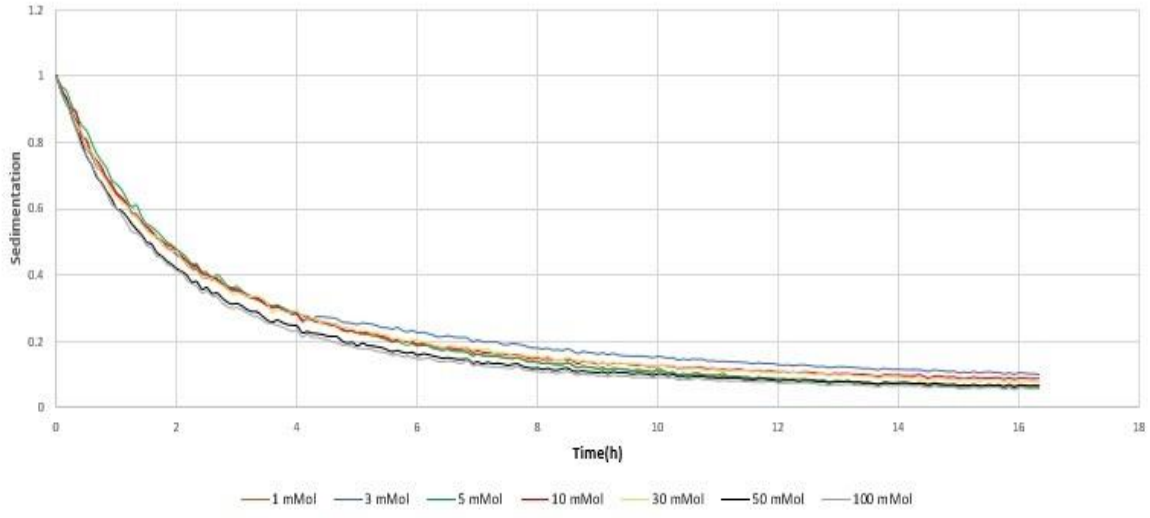

figure 4.25. Sedimentation over time for CAC 1g/l + mMol NaCl at different concentrations

All curves show a decreasing trend in concentration (C/C_0) over time, indicating that particles are settling out of suspension across all NaCl concentrations.

The sedimentation rates for NaCl concentrations 1 to 30 mMol are very similar, with all curves showing a consistent decline over time.

The sedimentation rates for the 50 mMol (black curve) and 100 mMol (gray curve) samples are slightly faster. This suggests that at high NaCl concentrations, particles become less stable and settle more quickly.

The calculated sedimentation half-time:

- 1 mMol: 1.7 hours
- 3 mMol: 1.72 hours
- 5 mMol: 1.8 hours
- 10 mMol: 1.72 hours
- 30 mMol: 1.75 hours
- 50 mMol: 1.58 hours
- 100 mMol: 1.42 hours

The 1-30 mMol NaCl solutions have similar half-times (between 1.7 and 1.8 hours). The 50 mMol and 100 mMol NaCl solutions show shorter half-times, indicating faster sedimentation compared to the lower concentrations. These shorter times suggest that higher NaCl concentrations lead to less stable suspensions, with particles settling more quickly.

After around 8 hours, all curves begin to level off, indicating that sedimentation has largely stabilized, and most particles have settled by this point. The lower NaCl concentrations (e.g., 1-10 mMol) exhibit higher final C/C_0 values, suggesting that more particles remain suspended in solution over time. The higher NaCl concentrations (50 mMol and 100 mMol) have lower final C/C_0 values, indicating that more particles have settled by the end of the experiment, which aligns with their faster sedimentation rates.

Figure 4.26 shows the half-time ($C/C_0 = 0.5$) in hours for sedimentation of 1 g/l concentration of CAC + mMol NaCl at different concentrations (ranging from 1 mM to 100 mM).

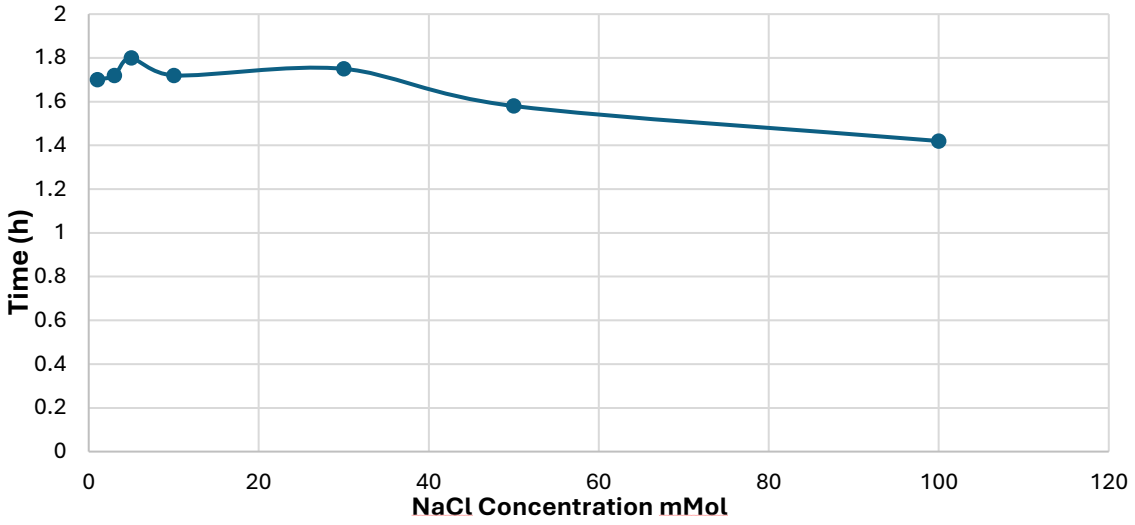

figure 4.26. Half-time for sedimentation of 1 g/l concentration of CAC + mMol NaCl at different concentrations

4.2.7. Column test

Figure 4.27 represents the breakthrough curve of CAC, that is, the normalized absorbance (A/A_0) over time during the column test conducted to evaluate the mobility of CAC through the column.

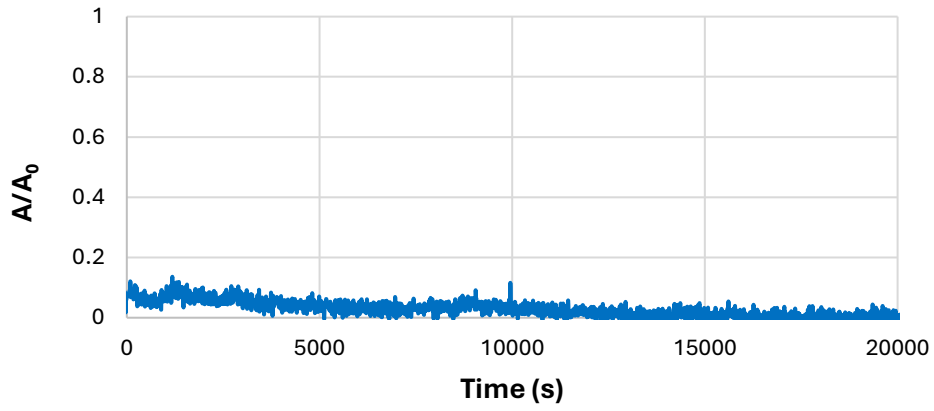

figure 4.27. Normalized absorbance (A/A_0) over time for column test

The normalized concentration remains below 0.1 during the entire test. This indicates a limited breakthrough due to strong retention of CAC within the column, likely due to sedimentation and mechanical filtration processes.

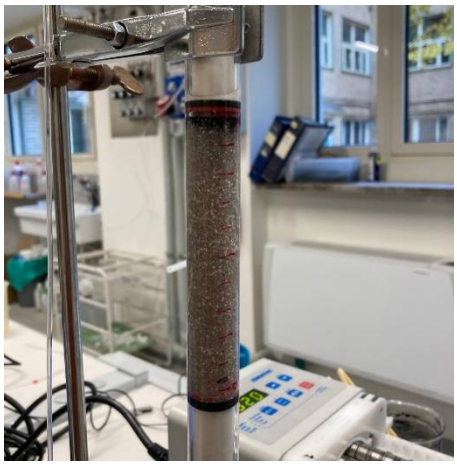

figure 4.28. Final result of column test

5. Conclusions

This thesis has explored the feasibility of using a commercial colloidal activated carbon (CAC) as an in-situ remediation agent to adsorb and immobilize BTEX in groundwater at petrochemical sites. The research revealed that CAC stability is compromised in saline conditions where particle aggregation and sedimentation were observed. Column tests further illustrated CAC's partial mobility —less than 10% was recovered at the outlet— within porous media, suggesting that while limited mobility in porous media may reduce its radius of influence upon injection, it minimizes re-mobilization risks, allowing for the sustained capture of BTEX within the treatment zone. This containment characteristic is critical, especially for complex sites where contaminants persist due to groundwater fluctuations and traditional methods like pump-and-treat or air sparging are impractical.

To evaluate CAC full potential in the field, further research is necessary to address key issues, particularly concerning injection strategies and long-term monitoring of CAC's retention and performance in variable hydrogeological conditions. Also, formulation adjustments to enhance stability across different groundwater conditions and refinement of injection methods to ensure adequate distribution in the target zone.

Ultimately, this thesis advances our understanding of CAC's use in BTEX remediation, offering a foundation for future work aimed at integrating CAC into comprehensive remediation programs for complex petrochemical sites.

Bibliography

"Air Sparging - an Overview | ScienceDirect Topics." n.d. Accessed November 4, 2024. https://www.sciencedirect.com/topics/earth-and-planetary-sciences/air-sparging.

Almeida, Francisclainy, Alecrícia Barros, Rosana Gonçalves Barros, Viníciu Bárbara, and Guilherme Lemos. 2019. "ÁREAS CONTAMINADAS POR POSTOS DE COMBUSTÍVEIS: UMA ABORDAGEM GERENCIAL." In .

Almpanis, Angelos, Lee Slater, and Christopher Power. 2024. "Monitoring Carbon-Based Remediation of DNAPL-Contaminated Groundwater via Spectral Induced Polarization." *Journal of Environmental Management* 368 (September):122111. https://doi.org/10.1016/j.jenvman.2024.122111.

Anjum, Hirra, Khairiraihanna Johari, Nirmala Gnanasundaram, Magesh Ganesapillai, Appusamy Arunagiri, Iyyaswami Regupathi, and Murugesan Thanabalan. 2019. "A Review on Adsorptive Removal of Oil Pollutants (BTEX) from Wastewater Using Carbon Nanotubes." *Journal of Molecular Liquids* 277 (March):1005–25. https://doi.org/10.1016/j.molliq.2018.10.105.

Ayotamuno, M. J., R. B. Kogbara, S. O. T. Ogaji, and S. D. Probert. 2006. "Petroleum Contaminated Ground-Water: Remediation Using Activated Carbon." *Applied Energy* 83 (11): 1258–64. https://doi.org/10.1016/j.apenergy.2006.01.004.

Bergler, Felix, Friedrich Schöppler, Frank Brunecker, Michael Hailman, and Tobias Hertel. 2013. "Fluorescence Spectroscopy of Gel-Immobilized Single-Wall Carbon Nanotubes with Microfluidic Control of the Surfactant Environment." *The Journal of Physical Chemistry C* 117 (June):13318–23. https://doi.org/10.1021/jp403711e.

Bhatnagar, Amit, William Hogland, Marcia Marques, and Mika Sillanpää. 2013. "An Overview of the Modification Methods of Activated Carbon for Its Water Treatment Applications." *Chemical Engineering Journal* 219 (March):499–511. https://doi.org/10.1016/j.cej.2012.12.038.

Bhattacharjee, Sourav. 2016. "DLS and Zeta Potential – What They Are and What They Are Not?" *Journal of Controlled Release* 235 (August):337–51. https://doi.org/10.1016/j.jconrel.2016.06.017.

Caetano, Marcelo, I. Schneider, Luciana Gomes, Amanda Kieling, and Luis Miranda. 2016. "A Compact Remediation System for the Treatment of Groundwater Contaminated with BTEX and TPH." *Environmental Technology* 38 (August):1–37. https://doi.org/10.1080/09593330.2016.1231222.

Carey, Grant R., Richard H. Anderson, Paul Van Geel, Rick McGregor, Keir Soderberg, Anthony Danko, Seyfollah Gilak Hakimabadi, Anh Le-Tuan Pham, and Mia Rebeiro-Tunstall. 2024. "Analysis of Colloidal Activated Carbon Alternatives for in Situ Remediation of a Large PFAS Plume and Source Area." *Remediation Journal* 34 (1): e21772. https://doi.org/10.1002/rem.21772.

Chen, Xiaowei, Nanjing Zhao, Wanjiang Zhu, Gaofang Yin, Renqing Jia, Ruifang Yang, and Mingjun Ma. 2025. "A New Method for the Rapid Identification of External Water Types in Rainwater Pipeline Networks Using UV–Vis Absorption Spectroscopy." *Spectrochimica Acta Part A: Molecular and Biomolecular Spectroscopy* 324 (January):124968. https://doi.org/10.1016/j.saa.2024.124968.

Ciampi, Paolo, Carlo Esposito, Ernst Bartsch, Eduard J. Alesi, and Marco Petrangeli Papini. 2023a. "Pump-and-Treat (P&T) vs Groundwater Circulation Wells (GCW): Which Approach Delivers More Sustainable and Effective Groundwater Remediation?" *Environmental Research* 234 (October):116538. https://doi.org/10.1016/j.envres.2023.116538.

———. 2023b. “Pump-and-Treat (P&T) vs Groundwater Circulation Wells (GCW): Which Approach Delivers More Sustainable and Effective Groundwater Remediation?” *Environmental Research* 234 (October):116538. https://doi.org/10.1016/j.envres.2023.116538.

Costa, A.S., L.P.C. Romão, B.R. Araújo, S.C.O. Lucas, S.T.A. Maciel, A. Wisniewski, and M.R. Alexandre. 2012. “Environmental Strategies to Remove Volatile Aromatic Fractions (BTEX) from Petroleum Industry Wastewater Using Biomass.” *Bioresource Technology* 105 (February):31–39. https://doi.org/10.1016/j.biortech.2011.11.096.

Eslami, Mahboubeh, Reza Khorassani, Massimo Coltorti, Daniele Malferrari, Barbara Faccini, Giacomo Ferretti, Dario Giuseppe, Amir Fotovat, and Akram Halajnia. 2017. “Leaching Behaviour of a Sandy Soil Amended with Natural and NH 4 + and K + Saturated Clinoptilolite and Chabazite.” *Archives of Agronomy and Soil Science* 64 (December). https://doi.org/10.1080/03650340.2017.1414944.

“Exchange Surfaces - Surface Areas to Volume Ratios (GCSE Biology).” n.d. *Study Mind* (blog). Accessed October 15, 2024. https://studymind.co.uk/notes/surface-areas-to-volume-ratios/.

Fayemiwo, Om & Daramola, M.O. & Moothi, Kapil. n.d. “BTEX Compounds in Water-Future Trends and Directions for Water Treatment.” *(2017)*, no. Water S.A. 43.

Fedele, Laura, Laura Colla, Sergio Bobbo, Simona Barison, and Filippo Agresti. 2011. “Experimental Stability Analysis of Different Water-Based Nanofluids.” *Nanoscale Research Letters* 6 (1): 300. https://doi.org/10.1186/1556-276X-6-300.

Georgi, Anett, Ariette Schierz, Katrin Mackenzie, and Frank-Dieter Kopinke. 2015a. “Colloidal Activated Carbon for In-Situ Groundwater Remediation — Transport Characteristics and Adsorption of Organic Compounds in Water-Saturated Sediment Columns.” *Journal of Contaminant Hydrology* 179 (August):76–88. https://doi.org/10.1016/j.jconhyd.2015.05.002.

———. 2015b. “Colloidal Activated Carbon for In-Situ Groundwater Remediation — Transport Characteristics and Adsorption of Organic Compounds in Water-Saturated Sediment Columns.” *Journal of Contaminant Hydrology* 179 (August):76–88. https://doi.org/10.1016/j.jconhyd.2015.05.002.

“GroundwaterEngineeringBook.Pdf.” n.d. Accessed November 15, 2024. http://amac.md/Biblioteca/data/28/14/10/23.2.pdf.

Han, Yongxiang, Yaqi Sheng, Jiating Zhao, and Lizhong Zhu. 2024. “Prediction of BTEX Volatilization in Polluted Soil Based on the Sorption Potential Energy Theory.” *Environmental Pollution* 360 (November):124624. https://doi.org/10.1016/j.envpol.2024.124624.

Hellmy, Muhamad, and Nur Azida. 2023. “Selective Visualization Techniques for Elemental Mapping Analysis of Granite Stones by Field Emission Scanning Electron Microscopy and Energy Dispersive Spectroscopy (FESEM-EDXS).” *Materials Today: Proceedings*, Innovative Manufacturing, Mechatronics & Material Forum 2022 (iM3F 2022), 75 (January):173–80. https://doi.org/10.1016/j.matpr.2022.11.315.

Heryanto, Heryanto, Dahlang Tahir, Bualkar Abdullah, Mustafa Kavgaci, Asnan Rinovian, Rachid Masrour, Venkata Siva Rama Prasad, and M.I. Sayyed. 2024. “Carbon as a Multifunctional Material in Supporting Adsorption Performance for Water Treatment: Science Mapping and Review.” *Desalination and Water Treatment* 320 (October):100758. https://doi.org/10.1016/j.dwt.2024.100758.

“Malvern Zetasizer Nano ZS ZEN3600 Size and Zeta Potential Particle Size +PC, S/W - SOLD.” n.d. Salford Scientific Supplies. Accessed October 16, 2024. https://salfordscientific.co.uk/shop/laboratory-balance-weighing-ph-meter-melting-point/malvern-zetasizer-nano-zs-zen3600-size-and-zeta-potential-particle-size-pc-s-w/.

McGregor, Rick. 2020. “Distribution of Colloidal and Powdered Activated Carbon for the <I>in Situ</I> Treatment of Groundwater.” *Journal of Water Resource and Protection* 12 (12): 1001–18. https://doi.org/10.4236/jwarp.2020.1212060.

Mishra, Raghvendra Kumar, Ajesh K. Zachariah, and Sabu Thomas. 2017. “Chapter 12 - Energy-Dispersive X-Ray Spectroscopy Techniques for Nanomaterial.” In *Microscopy Methods in Nanomaterials Characterization*, edited by Sabu Thomas, Raju Thomas, Ajesh K. Zachariah, and Raghvendra Kumar Mishra, 383–405. Micro and Nano Technologies. Elsevier. https://doi.org/10.1016/B978-0-323-46141-2.00012-2.

Molé, Rachel A., Adriana C. Velosa, Grant R. Carey, Xitong Liu, Guangbin Li, Dimin Fan, Anthony Danko, and Gregory V. Lowry. 2024. “Groundwater Solutes Influence the Adsorption of Short-Chain Perfluoroalkyl Acids (PFAA) to Colloidal Activated Carbon and Impact Performance for in Situ Groundwater Remediation.” *Journal of Hazardous Materials* 474 (August):134746. https://doi.org/10.1016/j.jhazmat.2024.134746.

Nguyen, Dung, and Charles E. Schaefer. 2023. “Application of Rapid, Small-Scale Column Tests to Assess Treatment of Perfluoroalkyl Acids in Groundwater Using A Novel Modified Clay Sorbent.” *Industrial & Engineering Chemistry Research* 62 (34): 13314–23. https://doi.org/10.1021/acs.iecr.3c02159.

Niarchos, Georgios, Linnea Georgii, Lutz Ahrens, Dan Berggren Kleja, and Fritjof Fagerlund. 2023. “A Systematic Study of the Competitive Sorption of Per- and Polyfluoroalkyl Substances (PFAS) on Colloidal Activated Carbon.” *Ecotoxicology and Environmental Safety* 264 (October):115408. https://doi.org/10.1016/j.ecoenv.2023.115408.

Noland, Scott, and Edward Winner. 2024. “Activated Carbon Injection for In-Situ Remediation of Petroleum Hydrocarbons.” In *Advances in the Characterisation and Remediation of Sites Contaminated with Petroleum Hydrocarbons*, edited by Jonás García-Rincón, Evangelos Gatsios, Robert J. Lenhard, Estella A. Atekwana, and Ravi Naidu, 549–89. Cham: Springer International Publishing. https://doi.org/10.1007/978-3-031-34447-3_16.

Oh, Min-Su, Geon Namgung, and Heonki Kim. 2024. “Enhanced Air Sparging for Groundwater Remediation Using Alginate Gel-Based Removable Hydraulic Barriers.” *Journal of Contaminant Hydrology* 260 (January):104258. https://doi.org/10.1016/j.jconhyd.2023.104258.

Panagos, Panos, Katrin Meusburger, Cristiano Ballabio, Pasquale Borrelli, and Christine Alewell. 2014. “Soil Erodibility in Europe: A High-Resolution Dataset Based on LUCAS.” *Science of The Total Environment* s 479–480 (May):189–200. https://doi.org/10.1016/j.scitotenv.2014.02.010.

“Petroleum Hydrocarbons.” n.d. *The Lake Simcoe Region Conservation Authority* (blog). Accessed November 16, 2024. https://lsrca.on.ca/index.php/home/petroleum-hydrocarbons-phcs/.

“PHC Testing.” n.d. *PPB Analytical Inc.* (blog). Accessed November 16, 2024. https://ppbanalytical.com/environmental-phc-testing/.

Pilaquinga, Fernanda, Jeroni Morey, Paulino Duel, Gabriela S. Yánez-Jácome, Esthefanía Chuisaca-Londa, Karen Guzmán, Jazel Caiza, et al. 2024. “Rapid, Low-Cost Determination of Hg2+, Cu2+, and Fe3+ Using a Cellulose Paper-Based Sensor and UV–Vis Method with Silver Nanoparticles Synthesized with *S. Mammosum*.” *Sensing and Bio-Sensing Research* 45 (August):100680. https://doi.org/10.1016/j.sbsr.2024.100680.

“PlumeStop-Remediation-Toronto-Canada.Pdf.” n.d. Accessed November 6, 2024. https://regenesis.com/wp-content/uploads/2019/01/PlumeStop-Remediation-Toronto-Canada.pdf.

“Products.” n.d. CPS Instruments. Accessed October 16, 2024. https://cpsinstruments.com/products/.

Raval, Nidhi, Rahul Maheshwari, Dnyaneshwar Kalyane, Susanne R. Youngren-Ortiz, Mahavir B. Chougule, and Rakesh K. Tekade. 2019. “Chapter 10 - Importance of Physicochemical Characterization of Nanoparticles in Pharmaceutical Product Development.” In *Basic Fundamentals of Drug Delivery*, edited by Rakesh K. Tekade, 369–400. Advances in Pharmaceutical Product Development and Research. Academic Press. https://doi.org/10.1016/B978-0-12-817909-3.00010-8.

“Remediation of Contaminated Sites-The Pump and Treat System | Wealthy Waste.” 2022. August 23, 2022. https://www.wealthywaste.com/remediation-of-contaminated-sites-the-pump-and-treat-system.

“Scanning Electron Microscopy.” n.d. Accessed October 16, 2024. https://nanoearth.ictas.vt.edu/content/nanoearth_ictas_vt_edu/en/access/selector/sem.html.

“Total Petroleum Hydrocarbons (TPH) | ToxFAQs™ | ATSDR.” n.d. Accessed November 16, 2024. https://wwwn.cdc.gov/TSP/ToxFAQs/ToxFAQsDetails.aspx?faqid=423&toxid=75.

“UV-Vis Spectroscopy: Principle, Strengths and Limitations and Applications.” n.d. Analysis & Separations from Technology Networks. Accessed October 16, 2024. http://www.technologynetworks.com/analysis/articles/uv-vis-spectroscopy-principle-strengths-and-limitations-and-applications-349865.

Wang, Bing, Chunyang Gao, Xingchun Li, Yuzhu Zhang, Tongxu Qu, Xianyuan Du, and Jin Zheng. 2022. “Remediation of Groundwater Pollution by in Situ Reactive Zone: A Review.” *Process Safety and Environmental Protection* 168 (December):858–71. https://doi.org/10.1016/j.psep.2022.10.046.

“Water-Solubility-and-Common-Concentrations-in-Gasoline-of-BTEX.Png (712×183).” n.d. Accessed November 4, 2024. https://www.researchgate.net/profile/Cleidiane-Zampronio/publication/238627987/figure/tbl2/AS:671537501855748@1537118425254/Water-solubility-and-common-concentrations-in-gasoline-of-BTEX.png.

“What Is the Z-Average? | Malvern Panalytical.” n.d. Accessed October 15, 2024. https://www.malvernpanalytical.com/en/learn/knowledge-center/faqs/faq0015averagediameter.

Wirthensohn, T., P. Schoeberl, U. Ghosh, and W. Fuchs. 2009. “Pilot Plant Experiences Using Physical and Biological Treatment Steps for the Remediation of Groundwater from a Former MGP Site.” *Journal of Hazardous Materials* 163 (1): 43–52. https://doi.org/10.1016/j.jhazmat.2008.06.053.

Woessner, William W., and Eileen P. Poeter. 2020. “5.3 Hydraulic Conductivity Values for Earth Materials,” August. https://books.gw-project.org/hydrogeologic-properties-of-earth-materials-and-principles-of-groundwater-flow/chapter/hydraulic-conductivity-values-for-earth-materials/.

“World Soil Day.” n.d. PK Climate Action. Accessed October 18, 2024. https://www.pkclimateaction.co.uk/event/world-soil-day-2.

Yu, Bian, Zhang Yuan, Zhou Yu, and Feng Xue-song. 2022. “BTEX in the Environment: An Update on Sources, Fate, Distribution, Pretreatment, Analysis, and Removal Techniques.” *Chemical Engineering Journal* 435 (May):134825. https://doi.org/10.1016/j.cej.2022.134825.

“Zeta Potential.” n.d. *Brookhaven Instruments* (blog). Accessed November 17, 2024. https://www.brookhaveninstruments.com/particle-characterization-applications/zeta-potential/.

Acknowledgements

At the end of this journey, my deepest gratitude goes to my beloved husband, Abbas, for his unwavering support and love, even across the distance and through all the challenges we faced. I am forever thankful to my wonderful family for their unexpected but deeply appreciated support, and to my dear friend Bahar, whose constant presence and help meant the world to me. My sincere thanks to Professor Tosco, whose endless patience, guidance, and knowledge were invaluable, and to dear Laura for her boundless support and kindness. A special thank you to Monica, whose steadfast encouragement helped me see this journey through to the end. Lastly, I am grateful to my dear Chrissy, whose inspiration carried me forward during my time at Arcadis.